

Unprecedented spring 2020 ozone depletion in the context of 20 years of measurements at Eureka, Canada

Kristof Bognar¹, Ramina Alwarda¹, Kimberly Strong¹, Martyn P. Chipperfield^{2,3}, Sandip S. Dhomse^{2,3}, James R. Drummond⁴, Wuhu Feng^{2,5}, Vitali Fioletov⁶, Florence Goutail⁷, Beatriz Herrera¹, Gloria L. Manney^{8,9}, Emily M. McCullough⁴, Luis F. Millán¹⁰, Andrea Pazmino⁷, Kaley A. Walker¹, Tyler Wizenberg¹, Xiaoyi Zhao⁶

¹Department of Physics, University of Toronto, Toronto, ON, Canada

²School of Earth and Environment, University of Leeds, Leeds, UK

³National Centre for Earth Observation, University of Leeds, Leeds, UK

⁴Department of Physics and Atmospheric Science, Dalhousie University, Halifax, NS, Canada

⁵National Centre for Atmospheric Science, University of Leeds, Leeds, UK

⁶Air Quality Research Division, Environment and Climate Change Canada, Toronto, ON, Canada

⁷LATMOS/IPSL, UVSQ Université Paris-Saclay, Sorbonne Université, CNRS, Guyancourt, France

⁸NorthWest Research Associates, Socorro, NM, USA

⁹Department of Physics, New Mexico Institute of Mining and Technology, Socorro, NM, USA

¹⁰Jet Propulsion Laboratory, California Institute of Technology, Pasadena, CA, USA

Key Points:

- Record low ozone columns (<200 DU) were observed over Eureka in spring 2020
- Limited dynamical resupply of ozone and chemical destruction both contributed to reduced ozone columns
- Mean chemical ozone loss of 111-127 DU (27-31%) represents similar absolute loss and greater relative loss compared to that in spring 2011

Corresponding author: K. Bognar, kbognar@atmosph.physics.utoronto.ca

Corresponding author: K. Strong, strong@atmosph.physics.utoronto.ca

Abstract

In the winter and spring of 2019/2020, the unusually cold, strong, and stable polar vortex created favorable conditions for ozone depletion in the Arctic. Chemical ozone loss started earlier than in any previous year in the satellite era, and continued until the end of March, resulting in the unprecedented reduction of the ozone column. The vortex was located above the Polar Environment Atmospheric Research Laboratory in Eureka, Canada (80 °N, 86 °W) from late February to the end of April, presenting an excellent opportunity to examine ozone loss from a single ground station. Measurements from a suite of instruments show that total column ozone in 2020 was at an all-time low in the 20-year dataset, 22 to 102 DU below previous records set in 2011. Ozone minima (<200 DU), enhanced OClO and BrO slant columns, and unusually low HCl, ClONO₂, and HNO₃ columns were observed in March. Polar stratospheric clouds were present as late as 20 March, and ozonesondes show unprecedented depletion in the March and April ozone profiles (to <0.2 ppmv). While both chemical and dynamical factors lead to reduced ozone when the vortex is cold, the contribution of chemical depletion was exceptional in spring 2020 when compared to typical Arctic winters. The mean chemical ozone loss over Eureka was estimated to be 111-127 DU (27-31%) using April measurements and passive ozone from the SLIMCAT chemical transport model. While absolute ozone loss was generally smaller in 2020 than in 2011, percentage ozone loss was greater in 2020.

Plain Language Summary

While an ozone hole forms over Antarctica every year, the Arctic typically doesn't experience such dramatic ozone loss. The chlorine and bromine (halogen) reactions that destroy ozone require very low temperatures that are rarely observed in the Arctic stratosphere. The winter and spring of 2019/2020, however, was unusually cold in the Arctic, and consequently, a large amount of ozone was destroyed by halogen chemistry. To understand the behaviour of ozone in spring 2020, we use measurements from the Polar Environment Atmospheric Research Laboratory in Eureka, Canada. Eureka (at 80 °N) is one of the northernmost research stations in the world, and thus an ideal location to observe ozone loss. Spring 2020 ozone minima were lower than any in the 20-year dataset, and ozone destruction was ongoing until the end of March, which is rare in the Arctic. While ozone concentrations are largely determined by circulation patterns in the Arctic stratosphere, chemistry in spring 2020 was a much larger factor than usual. Halogen chemistry destroyed 27-31% of the total ozone, compared to about 10% in a typical winter. The only year on record with comparable ozone loss is 2011, and a larger percentage of the ozone column was lost in 2020.

1 Introduction

During the spring of 2020, ozone loss in the Arctic stratosphere reached levels previously observed only in spring 2011 (Manney et al., 2020). Ozone loss was near complete at some altitudes, reminiscent of the Antarctic ozone hole (Wohltmann et al., 2020). Ozone depletion in the Arctic is typically less severe and more variable than in the Antarctic stratosphere, due to the large interannual variability of the Arctic polar vortex (e.g., WMO, 2018). The Arctic vortex is generally warmer, weaker, and more irregular, largely because of greater wave activity than in the Antarctic stratosphere. Combined with the significant impact of stratospheric dynamics on ozone variability (e.g., Tegtmeier et al., 2008), these conditions often generate a springtime column ozone maximum in the Arctic.

In order for significant chemical ozone loss to take place in the Arctic, the vortex needs to be strong and stable (undisturbed) throughout the winter and spring. The strong circulation isolates the air mass inside the vortex, and during the winter, temperatures can drop below the (pressure-dependent) thresholds for polar stratospheric cloud (PSC)

74 formation. HNO_3 might be incorporated into supercooled ternary solution (STS) droplets
75 or frozen nitric acid trihydrate (NAT) particles below ~ 195 K in the lower stratosphere
76 (Type I PSCs). Water ice particles form below ~ 188 K (Type II PSCs) (e.g., WMO, 2014).
77 PSCs (and other cold aerosols) then provide surfaces for the heterogeneous release of ac-
78 tive chlorine from its reservoir species, HCl and ClONO_2 (Solomon et al., 1986). PSCs
79 might also grow large enough to sediment, removing HNO_3 (a reservoir for NO_2) from
80 the stratosphere. This leads to the denitrification of the vortex, and hinders chlorine de-
81 activation via NO_2 (Salawitch et al., 1989; WMO, 2014). With the return of sunlight
82 in the spring, active chlorine is rapidly photolyzed, and ozone depletion proceeds through
83 the self-reaction of ClO (Molina & Molina, 1987) and the cross-reaction of ClO with BrO
84 (McElroy et al., 1986; Tung et al., 1986). In the absence of NO_2 to deactivate chlorine,
85 ozone loss can continue as long as the vortex remains cold and continues to act as a trans-
86 port barrier. The Arctic vortex, however, is often weak or already broken down by early
87 March (e.g., Manney, Santee, et al., 2011; Lawrence et al., 2018, and references therein),
88 preventing large-scale ozone depletion. For significant ozone loss to occur, the interplay
89 of several factors is required, such that the vortex becomes strong, cold, and long-lasting.

90 The winter of 2019/2020 stands as the best example of such conditions to date (e.g.,
91 Manney et al., 2020; Lawrence et al., 2020). While the size of the vortex was close to the
92 average for much of the winter, it maintained a more or less constant size to become one
93 of the largest by April. Potential vorticity (PV) gradients, a qualitative measure of the
94 vortex stability in the lower stratosphere, set all-time records from February to April,
95 indicating that the vortex acted as an exceptionally strong barrier to mixing and trans-
96 port (Lawrence et al., 2020). Temperatures inside the vortex remained below the thresh-
97 old for Type I PSCs (T_{NAT}) from early December to late March (the longest on record).
98 As a result, chlorine activation was apparent by late November, 2019, with high ClO con-
99 centrations persisting until the end of March (Manney et al., 2020). Lawrence et al. (2020)
100 argued that given the exceptional conditions outlined above, the winter of 2019/2020 had
101 the greatest ozone loss potential ever observed. While various methods of estimating ozone
102 loss have large uncertainties (e.g., Griffin et al., 2019; Manney et al., 2020), and dynam-
103 ical contributions to low ozone columns need to be considered (Tegtmeier et al., 2008),
104 measurements suggest that spring 2020 set new records for ozone depletion in the Arc-
105 tic. Minimum lower stratospheric ozone concentrations observed from satellites (Manney
106 et al., 2020) and ozonesondes (Wohlmann et al., 2020) were far smaller than previously
107 seen, approaching levels typical for the Antarctic ozone hole. Ozone columns were anoma-
108 lously low across the Arctic (Bernhard et al., 2020; Grooß & Müller, 2020; Inness et al.,
109 2020; Lawrence et al., 2020).

110 The previous winter with the most significant ozone loss was 2010/2011 (Balis et
111 al., 2011; Manney, Santee, et al., 2011; Sinnhuber et al., 2011; Adams, Strong, Zhao, et
112 al., 2012; Kuttippurath et al., 2012; Lindenmaier et al., 2012; Pommereau et al., 2013;
113 Strahan et al., 2013; Hommel et al., 2014; Solomon et al., 2014). The two seasons were
114 similar in many respects, with a persistent, strong, and cold vortex (Lawrence et al., 2020).
115 Ozone depletion, however, started later in 2010/2011 than in 2019/2020 (Manney et al.,
116 2020). In addition, the minimum ozone values in 2011 did not drop as low as in 2020,
117 and the minima occurred at higher altitudes. As a result, the total ozone column was
118 affected less in 2011 than in 2020 (Manney et al., 2020; Wohlmann et al., 2020). Esti-
119 mates of vortex-averaged chemical loss in the ozone column for 2011 vary based on the
120 methods, satellite instruments, and altitude ranges used, with reported values ranging
121 from 84-130 DU in the lower stratosphere (Sinnhuber et al., 2011; Kuttippurath et al.,
122 2012; Strahan et al., 2013) and 120-170 DU for the total column (Manney, Santee, et al.,
123 2011; Pommereau et al., 2013).

124 Significant Arctic ozone loss was also observed in the springs of 1996, 2000, and 2005
125 (Rex et al., 2004; Manney et al., 2006; Rex et al., 2006; Tilmes et al., 2006; Feng et al.,
126 2007). The vortex during these winters was particularly cold, but ozone depletion ceased

127 much earlier than in 2011 (Manney, Santee, et al., 2011) or 2020. The duration of the
128 cold period is key for large-scale ozone depletion, and the only year other than 2011 and
129 2020 with a large portion of the vortex below T_{NAT} going into March was 1997 (Coy
130 et al., 1997; Manney et al., 1997; Newman et al., 1997). The polar vortex in 1997 (along
131 with the vortex in 2020) was the largest on record for the March to early May period.
132 Temperatures below T_{NAT} persisted until late March, but the volume of cold air was
133 very limited until mid-January. This effectively delayed the depletion season by over a
134 month compared to 2019/2020. As a result, ozone loss in 1997 was less than in any of
135 the aforementioned years (Manney, Santee, et al., 2011). The 2015/2016 season started
136 with record-breaking low temperatures, the formation of ice PSCs, and significant de-
137 hydration of the vortex. An early final warming, however, broke up the vortex by early
138 March, preventing ozone loss on the scale of 2011 or 2020 (Manney & Lawrence, 2016;
139 Matthias et al., 2016; Johansson et al., 2019).

140 Given the large interannual variability of the polar vortex, long-term measurements
141 are necessary to assess stratospheric ozone depletion. Measurement stations in the Arc-
142 tic provide valuable data, but only when the vortex position is favorable. Here, we re-
143 port measurements from the Polar Environment Atmospheric Research Laboratory (PEARL)
144 (Fogal et al., 2013) in Eureka, Canada (80 °N, 86 °W). Measurements inside the spring
145 2011 vortex have been used in several studies to assess ozone depletion (Adams, Strong,
146 Zhao, et al., 2012; Lindenmaier et al., 2012; Adams et al., 2013; Pommereau et al., 2013),
147 and in 2020, the vortex was located above Eureka longer than in any previous year in
148 the measurement record. The datasets used here include long-term measurements of spring-
149 time trace gas columns from zenith-scattered-light differential optical absorption spec-
150 troscopy (ZSL-DOAS) instruments, a Fourier transform infrared (FTIR) spectrometer,
151 a Brewer spectrophotometer, and a Pandora spectrometer. In addition, we use measure-
152 ments from a Rayleigh-Mie-Raman lidar to identify PSCs, and simulations from the SLIM-
153 CAT chemical transport model to quantify chemical ozone loss.

154 This paper aims to assess the unprecedented spring 2020 ozone depletion in the con-
155 text of the 20-year time series from PEARL, with an emphasis on the similarities and
156 differences between 2020 and 2011. The paper is organized as follows: the datasets are
157 described in Section 2. The time series of ozone and other trace gases are discussed in
158 Section 3.1. Dynamical contributions to low ozone columns are examined in Section 3.2,
159 and estimates of chemical ozone loss are discussed in Section 3.3. Our conclusions are
160 given in Section 4.

161 2 Datasets and Methods

162 The DOAS and FTIR instruments used in this study are located in the PEARL
163 Ridge Lab (610 m asl). The Ridge Lab (known as the Arctic Stratospheric Ozone Ob-
164 servatory prior to 2005) is one of the three facilities that make up PEARL, and is op-
165 erated by the Canadian Network for the Detection of Atmospheric Change (CANDAC).
166 The Ridge Lab is located 15 km from the Environment and Climate Change Canada (ECCC)
167 Eureka Weather Station (EWS), while the other two PEARL facilities are within or near
168 EWS. PEARL is part of the Network for the Detection of Atmospheric Composition Change
169 (NDACC), and the ZSL-DOAS and Bruker FTIR instruments follow standards and best
170 practices outlined by the relevant NDACC working groups.

171 Springtime measurements at PEARL are supported by the Canadian Arctic ACE/OSIRIS
172 Validation Campaigns (Kerzenmacher et al., 2005), organized yearly since 2004. For the
173 purposes of this paper, we use data from the first measurement date to 5 May in each
174 year. Any yearly or overall averages refer to this period, unless specified otherwise. The
175 measurement periods, data products, and mean uncertainties for each instrument are shown
176 in Table 1, and the details are given in the following sections.

Table 1. Trace gas measurements used in this study, with mean relative uncertainties for each data product. Measurements up to 5 May in each year are included in the averages. The ozone and NO₂ products from the DOAS instruments (GBS, SAOZ) are 0-60 km total columns and 12-60 km partial columns, respectively. The BrO and OCIO products are dSCDs. Data products from the Bruker FTIR, Brewer and Pandora instruments are direct-sun total columns.

Instrument	Availability	Data products and mean uncertainty (%)						
		O ₃	NO ₂	BrO	OCIO	HCl	ClONO ₂	HNO ₃
GBS	1999–2020	6.3	20.2	26.0 ^a	24.2 ^a	–	–	–
SAOZ	2005–2020	5.9 ^b	13.9 ^b	–	–	–	–	–
Bruker FTIR	2007–2020	5.4	8.4	–	–	2.1	12.0	19.7
Brewer #69	2001–2020	0.5 ^c	–	–	–	–	–	–
Pandora	2019–2020	0.4 ^c	–	–	–	–	–	–

^aUV dSCDs (2007–2020), only including data over the detection limit

^bEstimates, see text

^cRandom uncertainty only, see text

2.1 ZSL-DOAS Measurements

The GBS (Ground-Based Spectrometer) dataset (ozone and NO₂) is comprised of measurements from two instruments, the University of Toronto GBS (UT-GBS) and the PEARL-GBS (Fraser et al., 2009). Both instruments are ultraviolet-visible (UV-vis) triple-grating spectrometers, with cooled charge-coupled device (CCD) detectors and a $\sim 1^\circ$ field-of-view. Springtime UT-GBS measurements are available for 1999-2020 (except for 2001 and 2002), and springtime PEARL-GBS measurements are available for 2007-2020. Since the two instruments are very similar and their measurements show excellent agreement, the datasets have been merged to create a single GBS dataset (Bognar et al., 2019). The SAOZ (Système d’Analyse par Observation Zénithale) instruments are part of a global network of similar instruments (Pommereau & Goutail, 1988). SAOZ instruments are UV-vis spectrometers with a fixed grating, an uncooled 1024-pixel linear photodiode array detector, and a $\sim 20^\circ$ field-of-view. The dataset is constructed from measurements of two identical instruments, SAOZ-15 (2005-2009) and SAOZ-7 (2010-2020) (Bognar et al., 2019).

The instruments utilize the DOAS technique (Platt & Stutz, 2008) to retrieve stratospheric trace gas concentrations. Differential slant column densities (dSCDs) of ozone were retrieved in the 450-550 nm wavelength range for both instruments. The NO₂ dSCDs were retrieved in the 425-490 nm range for the GBS dataset, while the SAOZ retrieval used 410-530 nm. The DOAS analysis for the GBS and SAOZ datasets differs in the use of daily and yearly reference spectra, respectively. The dSCDs were converted to vertical column densities using the retrieval settings recommended by the NDACC UV-vis Working Group (<http://ndacc-uvvis-wg.aeronomie.be/>, see also Hendrick et al., 2011). The ZSL-DOAS ozone columns represent ozone from the surface to 60 km (referred to as total columns), while ZSL-DOAS NO₂ columns are 12-60 km partial columns, as determined by the standard NDACC air mass factor look-up tables used in the retrievals. For a more detailed description of the ZSL-DOAS instruments and retrieval procedures, as well as comparisons of the GBS and SAOZ data, see Bognar et al. (2019).

In addition to ozone and NO₂ measurements in the visible range, the GBS instruments also measure in the UV. OCIO and BrO dSCDs were retrieved in the 350-380 nm and 345-359 nm ranges (Adams, Strong, Zhao, et al., 2012; Zhao, Strong, et al., 2016, respectively), using spectra averaged in 0.5° solar zenith angle (SZA) bins. The dSCDs were then averaged between 89° and 91° SZA. Based on the mean DOAS fitting error

and the standard deviation of dSCDs in the 89-91° SZA range, the 3σ detection limits were estimated to be 4.87×10^{13} molec cm⁻² for OCIO and 1.10×10^{14} molec cm⁻² for BrO. OCIO and BrO dSCDs are only reported when 90° SZA is available (until mid-April).

Uncertainty calculations for the ZSL-DOAS instruments are described in Bognar et al. (2019). The mean uncertainties for the measurement period (Table 1) are 6.3%, 20.2%, 24.2%, and 26.0% for the GBS ozone total columns, NO₂ partial columns, and OCIO and BrO dSCDs, respectively. The SAOZ uncertainties only include the DOAS fitting error. The total uncertainty of SAOZ ozone data was estimated to be 5.9% by Hendrick et al. (2011). SAOZ NO₂ measurements have an estimated precision of 1.5×10^{14} molec cm⁻² and accuracy of 10%. Combined in quadrature, this yields a total uncertainty of 13.9% for the SAOZ NO₂ measurements used here.

2.2 Direct-Sun Measurements

The CANDAC Bruker IFS 125HR Fourier transform infrared spectrometer (Bruker FTIR, Batchelor et al., 2009) measures solar absorption spectra using liquid-nitrogen cooled detectors (either a mercury cadmium telluride or an indium antimonide detector) and a potassium bromide beamsplitter. The measurements cover 600-4300 cm⁻¹ with a resolution of 0.0035 cm⁻¹. No apodization is applied to the measurements. Springtime Bruker FTIR measurements are available for 2007-2020.

The Bruker FTIR uses the SFIT4 version 0.9.4.4 retrieval algorithm (based upon the methods of Pougatchev et al., 1996) with the HITRAN 2008 spectroscopic line lists (Rothman et al., 2009) to retrieve volume mixing ratios of trace gases. SFIT4 uses optimal estimation to iteratively adjust the retrieved profiles to best fit the measured solar-absorption spectra (Rodgers, 2000). The ozone, HCl, ClONO₂, and HNO₃ retrievals use the settings recommended by the NDACC Infrared Working Group (<https://www2.acom.ucar.edu/irwg>), while NO₂ is currently not a standard NDACC product. The NO₂ retrieval settings are described in Bognar et al. (2019). For all of the retrievals, the a priori profiles are provided by 40-year average (1980-2020) profiles from the Whole Atmosphere Community Climate Model (WACCMv4, Eyring et al., 2007; Marsh et al., 2013), while daily pressure and temperature profiles used in the retrievals are provided by the U.S. National Centers for Environmental Prediction (NCEP). The retrievals are performed on a 47-layer grid (0.61 to 120 km), and only the integrated total columns are used here.

A full error analysis for all species was performed following Rodgers (2000). The uncertainties include smoothing error, forward model parameter error, and measurement noise error. Adding these in quadrature, the mean uncertainties for the retrieved total columns of ozone, NO₂, HCl, ClONO₂, and HNO₃ are 5.4%, 8.4%, 2.1%, 12.0%, and 19.7%, respectively (Table 1). For a detailed description of the error budget calculations, see Batchelor et al. (2009). The averaging kernels indicate that for each trace gas, the retrievals have good sensitivity to the lower stratosphere (Batchelor et al., 2009; Lindenmaier et al., 2012), with mean degrees of freedom for signal (DOFS) of 3.3, 1.3, 2.7, 1.1, and 2.7 for ozone, NO₂, HCl, ClONO₂, and HNO₃, respectively. Results for all species were filtered using an RMS:DOFS filter, and retrievals with negative volume mixing ratios (VMRs) were rejected. One exception is HCl, where negative VMRs were accepted in order to increase the number of valid measurements in low-HCl conditions (2011 and 2020). Negative VMRs rarely occur in retrievals for the other species.

Brewer spectrophotometers measure the intensity of direct sunlight in narrow wavelength bands in the UV range using a holographic grating (Kerr, 2002). Ozone total columns are calculated from relative intensities at 310.1, 313.5, 316.8, and 320 nm. The Brewer instruments have been designated as the World Meteorological Organization Global Atmosphere Watch standard ozone monitoring instrument since the 1980s, and more than 230 Brewers have been deployed to date (Zhao et al., 2020). While multiple Brewers are located in Eureka, only data from Brewer #69 is used here, since that instrument has

261 the longest dataset of all the Brewers that have measurements for 2020. Brewer #69 is
 262 a MKV single monochromator that took measurements from 2001 to 2020 from the roof
 263 of the EWS building. Ozone columns are calculated from an average of five successive
 264 measurements. To avoid straylight, which affects single Brewers at high SZA, data with
 265 air mass factors greater than 5 ($SZA > 79.5^\circ$) and standard deviations greater than 2.5
 266 DU were excluded. The random uncertainty of Brewer measurements was estimated to
 267 be 0.5% by Zhao et al. (2020), and the mean of the reported standard deviations in the
 268 filtered Brewer #69 dataset is 0.3%.

269 A Pandora spectrometer (#144) has been deployed at the PEARL Ridge Lab since
 270 February 2019. This instrument is the first Pandora spectrometer deployed in the polar
 271 regions (<https://www.pandonia-global-network.org/>). The Pandora instruments
 272 use a temperature-stabilized grating spectrometer and a CCD detector (Herman et al.,
 273 2009; Tzortziou et al., 2012). While Pandora #144 utilizes a combination of viewing ge-
 274 ometries (including direct-sun, direct-moon, zenith-sky, and multi-axis), only the direct-
 275 sun ozone measurements are used here. Other Pandora measurements at Eureka will be
 276 a subject of a separate study. The direct-sun spectra are analyzed using the total opti-
 277 cal absorption spectroscopy (TOAS) technique (Cede, 2019), and ozone is retrieved in
 278 the 310-330 nm range. The Pandora standard ozone column data products have a tem-
 279 perature dependence (Herman et al., 2015; Zhao, Fioletov, et al., 2016). This temper-
 280 ature dependence introduces a 1 to 3% seasonal bias between the Pandora and the Brewer
 281 standard data products (Zhao et al., 2020). Thus, the Pandora ozone data are corrected
 282 by an empirical method with the ozone-weighted effective temperature (Zhao, Fioletov,
 283 et al., 2016). The random uncertainty of Pandora ozone measurements was estimated
 284 to be 0.4% by Zhao, Fioletov, et al. (2016).

285 2.3 Additional Data Sets

286 The CANDAC Rayleigh-Mie-Raman Lidar (CRL) is a ground-based zenith-pointing
 287 lidar located at the Zero-altitude PEARL auxiliary laboratory (OPAL) at Eureka. The
 288 CRL transmits 532 nm and 355 nm light generated by separate, but co-aligned, Nd:YAG
 289 lasers. A 1 m telescope and eight photomultiplier tubes capture backscattered light at
 290 seven wavelengths: Rayleigh elastic channels at 532 nm, 532 nm with depolarization, and
 291 355 nm; Raman channels for molecular nitrogen at 387 and 607 nm and for water vapour
 292 at 408 nm; and Rotational Raman channels at 528 and 531 nm. A complete description
 293 of the original configuration of the CRL is available in Nott et al. (2012), and an updated
 294 description of the depolarization system is given in McCullough et al. (2017). The CRL
 295 focuses on tropospheric cloud and aerosol measurements at high temporal and vertical
 296 resolution (1 minute \times 7.5 metre; see McCullough et al., 2019). Binning the data (e.g.
 297 30 minute \times 150 m) allows the CRL to also provide data products well into the strato-
 298 sphere. The two elastic backscatter channels (532 nm and 355 nm) can be used to de-
 299 tect PSCs.

300 Ozonesondes are launched on a weekly basis from EWS (Tarasick et al., 2016). Dur-
 301 ing the intensive phase of the Canadian Arctic ACE/OSIRIS Validation Campaigns (2004-
 302 2020, typically early March), ozonesondes are launched daily, weather permitting. In ad-
 303 dition to providing information for the estimation of ozone loss, ozonesondes were used
 304 in the GBS retrievals (Bognar et al., 2019), and to initialize the photochemical box model
 305 used for NO₂ diurnal scaling (Sect. 3.1). Radiosondes are launched twice daily, weather
 306 permitting, from EWS. Radiosonde temperature profiles were used to verify that can-
 307 didate PSC cases identified by CRL (Sect. 3.1) were found within temperature regimes
 308 consistent with PSC formation: regions above the first tropopause, and with tempera-
 309 ture less than the threshold temperature for Type I PSC formation (T_{NAT}). The first
 310 tropopause was identified as the lowest altitude at which the lapse rate was less than 2
 311 K km⁻¹, and for which the average lapse rate over the following 2 km also did not ex-
 312 ceed 2 K km⁻¹ (WMO, 1957).

313 To select measurements inside the polar vortex, we used derived meteorological prod-
 314 ucts (DMPs) (Manney et al., 2007) from the second Modern-Era Retrospective analy-
 315 sis for Research and Applications (MERRA-2). MERRA-2 is an atmospheric reanaly-
 316 sis that utilizes the Goddard Earth Observing System Model Version 5.12.4 reanalysis
 317 system (GEOS-5) (GMAO, 2015; Gelaro et al., 2017). Values of scaled potential vortic-
 318 ity (sPV) (Dunkerton & Delisi, 1986; Manney et al., 1994) and temperature were cal-
 319 culated along the line-of sight of the ground-based instruments (for each individual mea-
 320 surement time), and vertically for SLIMCAT columns and radiosondes, using the Jet and
 321 Tropopause Products for Analysis and Characterization (JETPAC) package (Manney,
 322 Hegglin, et al., 2011). The line-of-sight calculations for the ZSL-DOAS instruments are
 323 described in Adams, Strong, Batchelor, et al. (2012). It should be noted that unlike for
 324 direct-sun measurements, exact line-of-sight calculations are not possible for the ZSL-
 325 DOAS instruments, due to the multiple paths taken by scattered sunlight before reach-
 326 ing the detectors. The approximate nature of the ZSL-DOAS DMPs, combined with the
 327 long integration times corresponding to each vertical column (2-4 hours, 30-60° change
 328 in the solar azimuth), means the ZSL-DOAS results should be interpreted with caution
 329 when the vortex edge is near Eureka.

330 For the purposes of this study, the inner edge of the vortex was defined as $\text{sPV} =$
 331 $1.6 \times 10^{-4} \text{ s}^{-1}$, and the outer edge as $\text{sPV} = 1.2 \times 10^{-4} \text{ s}^{-1}$ (Manney et al., 2007). To fil-
 332 ter out measurement that potentially sample through the vortex edge, sPV criteria were
 333 tested at 16, 18, and 20 km (the altitude range of maximum ozone concentrations) along
 334 the line-of-sight of each instrument. Measurements were considered to be inside (out-
 335 side) the vortex if the sPV at all three altitudes was greater (less) than the inner (outer)
 336 vortex edge threshold. Measurements not matching these criteria were assumed to be
 337 on the vortex edge and were excluded from the analysis in this paper.

338 To investigate ozone loss inside the vortex, we use output from the TOMCAT/SLIMCAT
 339 (hereafter SLIMCAT) three-dimensional offline chemical transport model (Chipperfield,
 340 2006; Dhomse et al., 2013; Chipperfield et al., 2015; Dhomse et al., 2019). The model
 341 is forced by ERA5 analyses provided by the European Centre for Medium-Range Weather
 342 Forecasts (Hersbach et al., 2020), and the chemistry component is performed separately
 343 for each time-step. SLIMCAT includes both active ozone, for which the full chemistry
 344 and dynamics are considered, and passive ozone, which is dynamical tracer with no chem-
 345 istry. Passive ozone is set equal to active ozone on 1 December of each year. Passive ozone
 346 can be used to estimate chemical ozone loss as the difference between passive and ac-
 347 tive (or measured) ozone (e.g., Feng et al., 2007; Singleton et al., 2005, 2007; Adams, Strong,
 348 Zhao, et al., 2012; Lindenmaier et al., 2012; Dhomse et al., 2013). Here we use 6-hourly
 349 model output for 2000-2020, interpolated to the geolocation of Eureka. Column values
 350 were calculated from trace gas VMR profiles using modeled pressure and temperature
 351 profiles.

352 **3 Results and Discussion**

353 **3.1 The Spring 2020 Measurements in Context**

354 The polar vortex was located above or near Eureka for much of spring 2020. All
 355 instruments sampled continuously inside the vortex from 25 February through 31 March.
 356 Before that, the earliest SAOZ measurements (20-22 February) were inside the vortex,
 357 and the ZSL-DOAS instruments sampled through the vortex edge on 23-24 February.
 358 In April and May, the vortex location was more variable. The instruments measured in-
 359 side the vortex for 9-18 and 27-30 April, mostly through the vortex edge for 1-7 and 19-
 360 26 April, and on the edge or outside the vortex from 1 May on. The exceptional longevity
 361 of the vortex (Lawrence et al., 2020) is evidenced by the fact that 30 April is the latest
 362 in-vortex measurement (by two weeks) in the 20-year dataset presented here. It should
 363 be noted that the number of in-vortex measurements depends on the location of the vor-

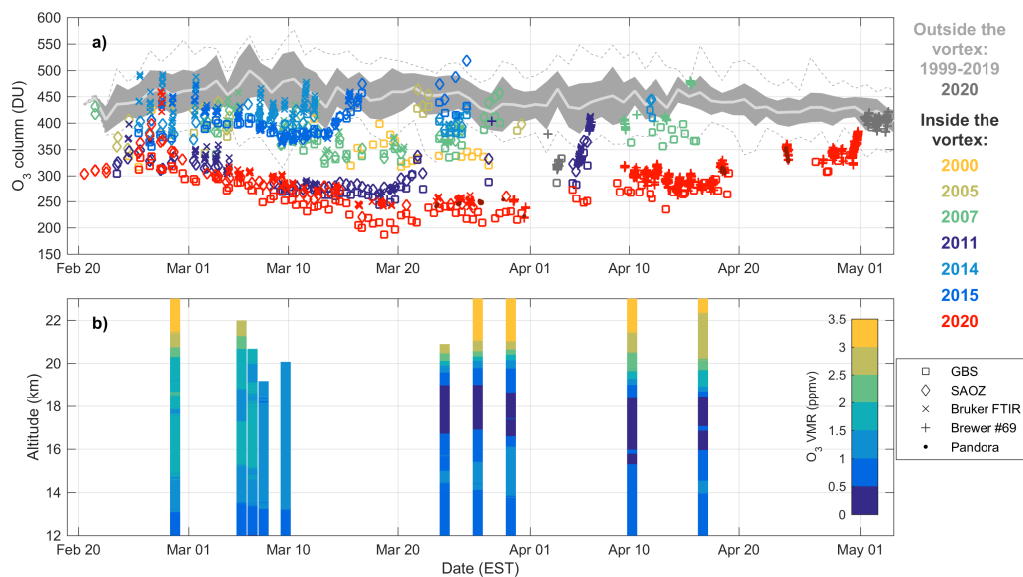


Figure 1. a) Measurements of total column ozone (DU) from the GBS, SAOZ, Bruker FTIR, Brewer, and Pandora instruments. Measurements outside the vortex in the time series of all instruments (up to 2019) are represented by the gray shaded area (daily mean and standard deviation) and the gray dashed lines (daily minima and maxima). The colored datapoints represent measurements inside the vortex, in years when the vortex was located above Eureka for a substantial part of the measurement period. In addition, 2020 measurements outside the vortex are plotted separately in dark gray. b) Ozone mixing ratio profiles (ppmv) from 2020 ozonesonde measurements. Only sondes that reached altitudes above 18 km are shown.

364 tex, and also on the measurement coverage of the individual instruments. Direct-sun mea-
 365 surements require clear conditions, and unfavorable weather can significantly reduce mea-
 366 surement coverage, especially for the early spring (high SZA). ZSL-DOAS instruments,
 367 on the other hand, measure in cloudy conditions as well, but provide data for twilights
 368 only. Measurements in 2020 faced additional challenges as a result of the COVID-19 pan-
 369 demic. The Bruker FTIR and SAOZ measurements ended on 26 and 30 March, respec-
 370 tively, due to lack of on-site support. GBS measurements, however, continued for the rest
 371 of the spring, and Brewer #69 measurements (which typically start in late March) pro-
 372 vided direct-sun data for the rest of the spring. Pandora direct-sun measurements are
 373 limited to a few days in spring 2020, due in part to the lack of on-site support.

374 Figure 1a shows measurements of ozone columns inside and outside the vortex for
 375 the full time series of all instruments. The 2020 measurements are exceptional, both con-
 376 sidering the duration of in-vortex measurements, and the record low ozone columns. Ozone
 377 values inside the vortex show a clear decline through March, and all instruments recorded
 378 the all-time lowest values in their respective time series in the second half of March 2020.
 379 The GBS time series has the best coverage in spring 2020, and the lowest ozone values
 380 appear in this dataset, with ozone columns near or below 200 DU (minimum of 187 DU)
 381 for 16-19 March. SAOZ measurements show a minimum (221 DU) on March 16, although
 382 SAOZ has no measurements for 17-19 March. Bruker FTIR ozone columns were in the
 383 240-250 DU range for 16-19 March, while the minimum value (240 DU) was reached on
 384 26 March. The GBS and SAOZ instruments also measured column values between 210
 385 and 250 DU in late March. The Brewer and Pandora datasets start on 30 and 23 March,

386 respectively, and the minimum values (218 DU and 222 DU, respectively) were measured
387 on 31 March for both instruments. The scatter between the various instruments is ex-
388 pected, and the GBSs generally measure the least ozone among the various instruments
389 (Adams, Strong, Batchelor, et al., 2012; Bogner et al., 2019). The GBS and Brewer time
390 series continue (with good coverage) through April and early May, and show the grad-
391 ual increase of ozone inside the vortex. The vortex was still strong (and ozone columns
392 inside were still below background levels) by the end of April.

393 The decline of ozone columns inside the vortex in early March was similar to that
394 in 2011, the only previous year with comparable ozone columns in the dataset. Minimum
395 values in 2020, however, were much lower than those observed in 2011. GBS, SAOZ, and
396 Bruker FTIR measurements all reached their minima on 18 March 2011. In 2020, min-
397 imum ozone columns measured by the same instruments were lower by 56, 43, and 22
398 DU, respectively. Minimum ozone in the Brewer dataset was 102 DU lower in 2020 than
399 in 2011, although Brewer #69 generally has few measurements inside the vortex. While
400 the vortex moved away from Eureka in late March of 2011, there is no indication that
401 ozone columns reached minima similar to 2020. Other years when the vortex spent a sig-
402 nificant amount of time above Eureka do not show ozone columns comparable to 2011
403 and 2020 (nearest minima are 93-143 DU higher than the lowest 2020 values). Ozone sup-
404 ply, however, is variable from year to year (e.g., Tegtmeier et al., 2008), and a cold strato-
405 sphere generally corresponds to reduced ozone columns even without chemical depletion.
406 Part of the record low column ozone in 2020 is likely related to dynamics, and this is ex-
407 amined further in Section 3.2.

408 Figure 1b shows ozone profiles measured by ozonesondes in spring 2020. The grad-
409 ual depletion of ozone in the 16-20 km altitude range is apparent by early March, and
410 the same altitude range shows exceptionally low mixing ratios in late March and April.
411 Mixing ratios were consistently below 0.5 ppmv in a wide altitude range (with minima
412 below 0.2 ppmv), indicating near-complete depletion of ozone. Such low values are un-
413 precedented in the Arctic: even in 2011, mixing ratios did not drop below 0.5 ppmv (e.g.,
414 Solomon et al., 2014). Ozonesonde profiles from other Arctic sites paint a consistent pic-
415 ture of ozone depletion that is unprecedented in the Arctic, and is more similar to Antarc-
416 tic winters than any previously observed Arctic winter (Wohltmann et al., 2020). The
417 altitude of the depleted layer likely explains some of the differences between the column
418 measurements in Figure 1a. Estimated scattering heights for ZSL-DOAS instruments are
419 below 16 km (Adams, Strong, Batchelor, et al., 2012). As a result, path lengths in the
420 16-20 km altitude range are several times longer for ZSL-DOAS instruments than for direct-
421 sun measurements. The increased sensitivity to the region of depleted ozone likely con-
422 tributes to the lower ozone columns measured by the ZSL-DOAS instruments.

423 Figure 2 shows complementary measurements from the GBSs and Bruker FTIR,
424 along with temperatures from DMPs and radiosondes. BrO and OCIO dSCDs retrieved
425 from GBS measurements (Fig. 2a-b) were significantly above background levels in 2020.
426 This indicates ongoing chlorine activation from the earliest measurements (5 March) to
427 late March, with occasional enhancements in early April. BrO and OCIO enhancements
428 in 2011 were similar to 2020, although the 2011 time series is much shorter. There are
429 no other years in the data record with persistent enhancements of both BrO and OCIO.
430 The highest BrO dSCDs were recorded in 2015, but these correspond to smaller OCIO
431 enhancements (and much higher ozone columns) than either 2011 or 2020.

432 Extremely low values of chlorine reservoirs HCl and ClONO₂ in the Bruker FTIR
433 dataset (Fig. 2c-d) are consistent with the elevated OCIO values in the GBS data, and
434 indicate chlorine activation and heterogeneous chemistry on PSCs. HCl column values
435 were consistently very low in March, with the exception of a few measurements in late
436 February. ClONO₂ measurements follow the same pattern, with an additional minor peak
437 mid-March. Both HCl and ClONO₂ show a gradual recovery from approx. 20 March to
438 the end of the Bruker FTIR measurements (26 March). This increase corresponds to a

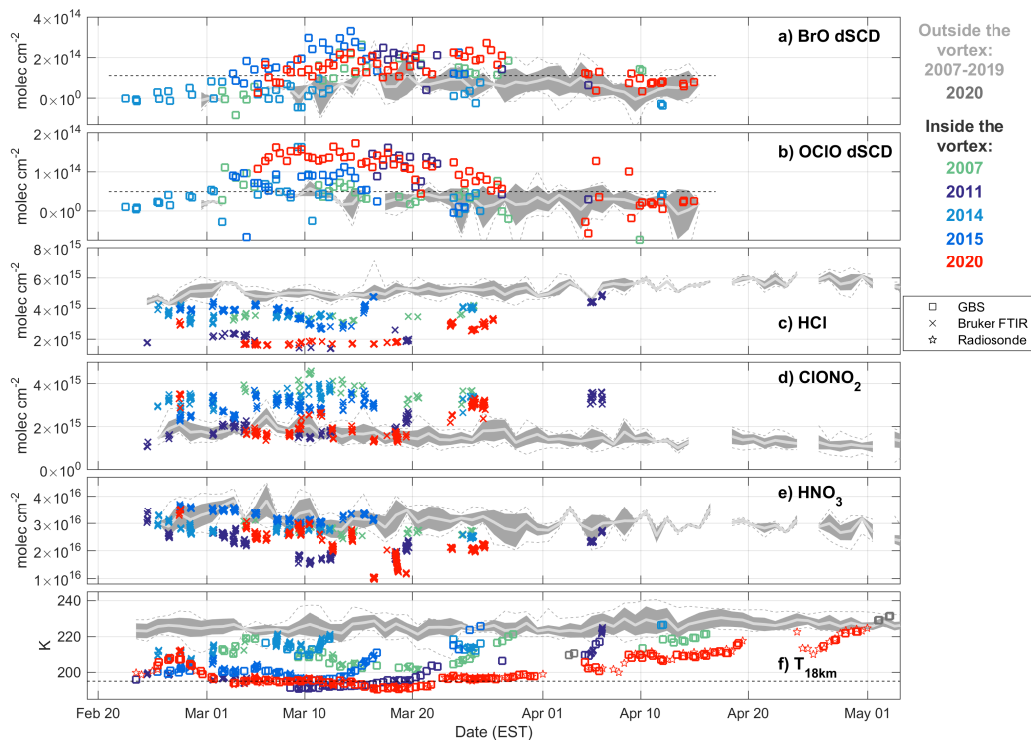


Figure 2. a) and b) Twilight measurements of BrO and OCIO dSCDs from the GBS dataset. The approximate detection limits are indicated by the dashed lines. c) to e) Measurements of HCl, ClONO₂, and HNO₃ columns from the Bruker FTIR. f) Temperature at the 18 km level along the line of sight of the Bruker FTIR and GBS instruments, as well as T_{18km} from 2020 radiosonde measurements. The dashed line indicates T_{NAT} (195 K). Plot colors and shading as in Fig. 1a.

439 gradual decrease in the OCIO dSCDs, consistent with conversion of active chlorine back
 440 into its reservoir species. These observations are generally consistent with satellite mea-
 441 surments of HCl and ClONO₂ presented by Manney et al. (2020). 2011 data tell a simi-
 442 lar story, with low HCl and ClONO₂ column values into March, and a gradual recov-
 443 ery in late March. HCl values dropped slightly lower in 2011 than in 2020, whereas for
 444 ClONO₂, the all-time minima were measured in 2020. ClONO₂ recovery started later
 445 in 2020, likely due in part to the slow increase of NO₂ concentrations (Fig. 4). In the
 446 rest of the measurement record, HCl and ClONO₂ show a marked decrease only in 2015,
 447 consistent with moderate enhancements of OCIO.

448 While low HCl and ClONO₂ columns point to the presence of PSCs, HNO₃ (the
 449 main component of Type I PSCs) was not exceptionally low in the early spring of 2020
 450 (Fig. 2e). HNO₃ remained close to typical background values until the second half of March.
 451 On 16-19 March, however, HNO₃ columns dropped to the lowest values by far in the Bruker
 452 FTIR data record. Lower stratospheric temperatures from radiosondes and along the line-
 453 of-sights of the GBS and Bruker FTIR measurements (Fig. 2f) show that the same mid-
 454 March period saw the lowest temperatures in 2020. T_{18km} was well below T_{NAT}, cre-
 455 ating prime conditions for PSC formation. ClONO₂ values reached their minimum in
 456 this cold period, but there was no discernible increase in the OCIO dSCDs. Ozone columns
 457 also reached their minima on 16-19 March. CRL data indicate the presence of PSCs over

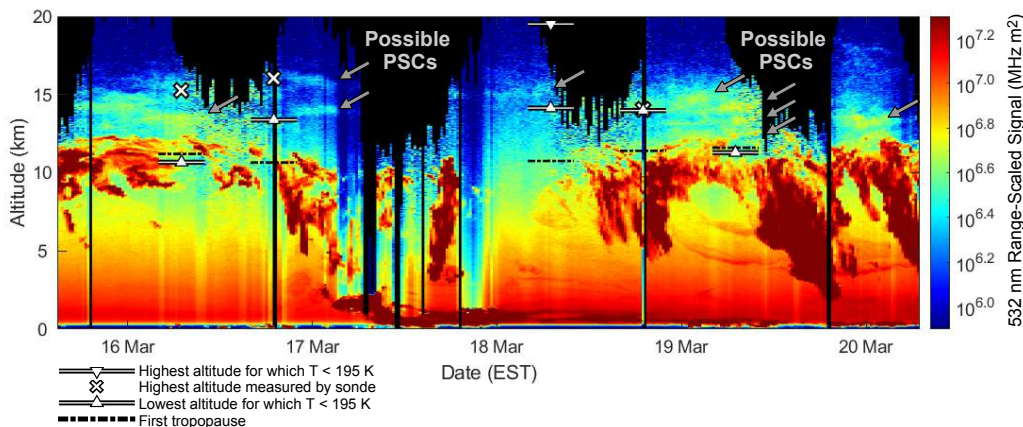


Figure 3. 532 nm range-scaled signal from the CRL for 16-20 March, during a period of PSC activity. Possible PSCs are particularly clear on 17 March as distinct features (~ 0.5 km vertical extent) at 14 and 16 km, which are brighter than surrounding areas by a factor of approximately 2.5. Other regions showing possible PSCs are visible on 16-20 March, above 12 km. As per radiosonde temperature profiles, the PSC regions are all above the first tropopause (dot-dashed black lines; see text), and also have temperatures below T_{NAT} (195 K, lines with upward triangles). Black areas indicate low signal-to-noise ratios, generally due to the high solar background during daytime, and occasionally due to attenuation of the laser beam by tropospheric features below 12 km.

458 Eureka during 16-20 March. Figure 3 shows the 532 nm attenuated backscatter coefficient
 459 from the CRL for the 0-20 km altitude range. The features between 12 and 16 km
 460 that are narrow in their altitude extent are most likely PSCs. These are particularly vis-
 461 ible on 17 March at 14 km and 16 km, again on 18 March at 15 km, and present on 16
 462 and 18 March at 13 km through 16 km. These features return signals brighter than the
 463 surrounding molecular background by a factor of approximately 2.5. In early March, tem-
 464 peratures hovered near (but generally above) T_{NAT} , consistent with the higher HNO_3
 465 values observed by the Bruker FTIR. Accordingly, there are no PSC candidates detected
 466 in March CRL data before 16 March. Coincident high OCIO values and low HCl and
 467 ClONO_2 columns indicate that PSCs were likely present elsewhere in the vortex (as shown
 468 by DeLand et al., 2020, for example), and the discrepancies are likely explained by the
 469 different time-scales for vortex mixing (~ 5 -7 days) and chlorine deactivation (weeks) (e.g.,
 470 Adams, Strong, Zhao, et al., 2012). It should be noted that the vertical distribution of
 471 HNO_3 was different in 2011 and 2020, and HNO_3 values were anomalously high before
 472 PSC formation started in 2019/2020 (Manney et al., 2020).

473 From mid-March into April, the 2020 vortex was the coldest among any year with
 474 measurements inside the vortex. Temperatures remained near T_{NAT} until the end of March,
 475 and only reached background values by the end of April. This slow warming correlates
 476 with the slow increase of ozone inside the vortex, as examined further in Section 3.2. While
 477 the vortex temperatures hovered around T_{NAT} for the entire month of March, the first
 478 observations in 2020 reveal higher temperatures in late February. This increase corre-
 479 sponds to peaks in the HCl , ClONO_2 and HNO_3 data. DMPs show that these measure-
 480 ments were taken near the vortex edge. The potential impact of mixing through the vor-
 481 tex edge manifests as an increase of the ozone and NO_2 columns (Figs. 1 and 4), as well
 482 as an increase in SLIMCAT passive ozone in the vortex (Sect. 3.3). Temperatures fol-
 483 lowed a different pattern in 2011. The lowest temperatures were observed around 10 March,
 484 T_{18km} increased gradually to early April, and then increased rapidly as the vortex moved

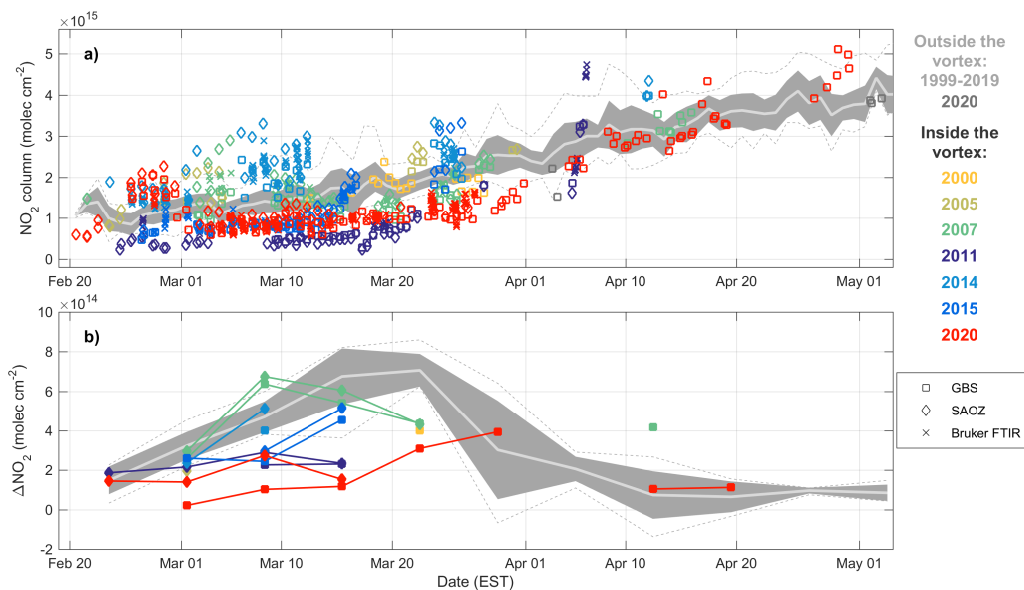


Figure 4. a) Measurements of NO₂ partial columns from the GBS and SAOZ instruments, and NO₂ total columns from the Bruker FTIR. The columns have been scaled to local noon. b) Weekly mean diurnal variability (evening minus morning) of NO₂ in the GBS and SAOZ measurements (without scaling). Mean values were calculated only if at least three daily values were available. Plot colors and shading as in Fig. 1a.

485 away from Eureka. Accordingly, HNO₃ measurements in mid-March were much lower
 486 in 2011 than in 2020. Chlorine reservoirs and OCIO, on the other hand, show similar be-
 487 haviour in both years, indicating the role of mixing in the vortex. Temperatures in 2015
 488 were also quite low, hovering near T_{NAT} in March. The cold conditions did not last, how-
 489 ever, and T_{18km} increased rapidly after 12 March.

490 NO₂ columns from the ZSL-DOAS instruments and the Bruker FTIR are shown
 491 in Figure 4a. To account for the diurnal variation of NO₂, partial columns were scaled
 492 to local noon using a photochemical box model (McLinden et al., 2000; Brohede et al.,
 493 2007). For more details on the scaling procedure, see Bognar et al. (2019) and Adams,
 494 Strong, Batchelor, et al. (2012). Aside from the peak in late February discussed above,
 495 NO₂ columns were generally low in 2020. Unlike other trace gases, NO₂ measurements
 496 did not reach record lows in early spring: in-vortex NO₂ in 2011 was consistently below
 497 2020 values. The 2020 measurements are consistent with the higher HNO₃ column val-
 498 ues measured by the Bruker FTIR (Fig. 2e). The mean diurnal increase of NO₂, on the
 499 other hand, was at its all-time minimum in both the GBS and SAOZ datasets in 2020
 500 (Fig. 4b, no diurnal scaling). As a result, the usual seasonal recovery of NO₂ concen-
 501 trations in the vortex proceeded much more slowly than in any other year in the mea-
 502 surement record, and NO₂ column values remained unseasonably low into late March.
 503 The diurnal increase of NO₂ only returned to background values in late March, coinci-
 504 dent with the increase of ClONO₂ values (Fig. 2d). A minor (and temporary) NO₂ in-
 505 crease after 10 March corresponds to the ClONO₂ peak discussed earlier, and it is likely
 506 related to mixing and transport, as opposed to local chemistry. In 2011, NO₂ columns
 507 were consistently lower than in 2020, but the diurnal increase was slightly above 2020
 508 values. NO₂ concentrations recovered rapidly during the 2011 vortex breakup (Adams
 509 et al., 2013), while the increase was more gradual in 2020. The only other year with con-

510 sistically low in-vortex NO_2 was 2015, but NO_2 values increased rapidly in mid-March,
 511 following similar trends in temperature and other trace gases. In other years, NO_2 in the
 512 vortex was generally above background levels.

513 In summary, all instruments used in this study measured record low ozone column
 514 values in spring 2020. The GBS, SAOZ, and Bruker FTIR instruments all measured the
 515 smallest (or close to the smallest) ozone columns (187-240 DU) in their respective time
 516 series on 16-19 March, well below 2011 minima. The same late March period also saw
 517 very low values of chlorine reservoirs HCl and ClONO₂, alongside temperatures below
 518 T_{NAT} , and an extraordinary drop in HNO₃ concentrations. These observations indicate
 519 the presence of PSCs (confirmed by CRL observations), and, combined with elevated OCIO
 520 and BrO dSCDs, point to significant chemical ozone depletion. Ozone profiles later
 521 in March (and well into April) showed unprecedented depletion of ozone in the 16-20 km
 522 altitude range, with mixing ratios below 0.2 ppmv. While the vortex was cold through-
 523 out the spring, $T_{18\text{km}}$ was consistently above T_{NAT} in the early spring, and again past
 524 21 March. HCl, ClONO₂, and NO_2 gradually recovered by late March, and OCIO dSCDs
 525 decreased below the detection limit. This indicates that chemical ozone loss inside the
 526 vortex likely stopped by the end of March (perhaps slightly later than in 2011). The vor-
 527 tex above Eureka appeared less denitrified in 2020 than in 2011, consistent with higher
 528 HNO₃ columns in 2020. Ozone columns in 2020 remained well below seasonal averages
 529 until the end of April. Dynamical and chemical contributions to these record low ozone
 530 columns are discussed in the following sections.

531 3.2 The Impact of Dynamics

532 Accurate assessment of chemical ozone depletion in the Arctic is hindered by the
 533 fact that dynamical and chemical contributions to low ozone columns are difficult to sep-
 534 arate. Approximately half of the variability in springtime ozone is due to interannual dif-
 535 ferences in ozone replenishment from above (Chipperfield & Jones, 1999; Tegtmeier et
 536 al., 2008). Since this replenishment is due to diabatic descent, resupply of ozone is gen-
 537 erally smaller in cold winters, when diabatic descent is weaker. Mixing through the vor-
 538 tex edge also contributes to ozone variability, and less mixing in cold winters contributes
 539 to reduced ozone columns, especially in March (Salby & Callaghan, 2007). These fac-
 540 tors (among others, see e.g., supplementary information of Manney, Santee, et al., 2011,
 541 and references therein) result in a good correlation between ozone and lower stratospheric
 542 temperature inside the vortex. On the other hand, since PSC formation is temperature-
 543 dependent, chemical ozone depletion also leads to a good correlation between ozone and
 544 temperature (e.g., Tilmes et al., 2006; Rex et al., 2006). The exact correlation, however,
 545 will depend on the balance of contributing factors, and so we might expect to see dif-
 546 ferent relationships between ozone and temperature depending on the relative impor-
 547 tance of chemistry and dynamics.

548 Figure 5 shows the relationship of in-vortex ozone columns and $T_{18\text{km}}$ for the GBS,
 549 SAOZ, Bruker FTIR, and Brewer datasets. The black dots and black dashed lines show
 550 the correlation for what might be considered 'typical' springtime conditions. These years
 551 (including early measurements in 2011 and 2020) all experienced a similar balance of chem-
 552 ical depletion and dynamical factors. The R^2 values are similarly high for all datasets,
 553 and the slopes vary only slightly, in accordance with the differences between ozone columns
 554 from each instrument. Even the limited number of points for the Brewer follow this cor-
 555 relation. Measurements from 2015 follow a different correlation, indicated by the gray
 556 dots and gray dashed lines in Figure 5. The slopes are approximately parallel to the cor-
 557 relation for typical years discussed above, but with a significant positive offset. R^2 val-
 558 ues are also high, but with more variability between the instruments. As shown in Fig-
 559 ures 1a and 2f, 2015 was a relatively cold year with anomalously high ozone. The rea-
 560 sons for this are examined in detail by Manney et al. (2015). A minor warming in Jan-
 561 uary 2015 caused unusually strong descent and high ozone values, with minimal chem-

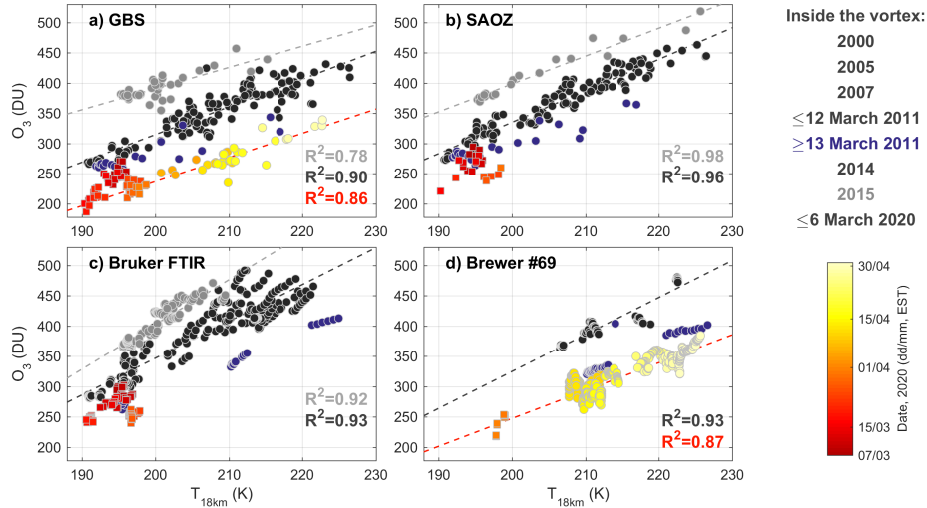


Figure 5. Ozone columns inside the vortex as a function of T_{18km} for **a)** the GBS, **b)** SAOZ, **c)** Bruker FTIR, and **d)** Brewer. In-vortex measurements for 'typical' years (alongside measurements from early spring 2011 and 2020) are shown in black, with a corresponding linear fit and R^2 value. In-vortex measurements for 2015 (and the corresponding linear fits and R^2 values) are plotted in gray. Measurements that start to deviate from the typical correlation (black dashed line) are plotted in blue for 2011, and with a color scale representing dates for 2020. For 2020, squares and dots correspond to March and April data, respectively. The red dashed lines show the linear fit for April 2020.

562 ical ozone destruction. It is then reasonable that the correlation of ozone and temper-
 563 ature would be different from typical years, since the contribution of chemical depletion
 564 was largely absent in 2015, tipping the balance towards the dynamical factors.

565 Measurements in spring 2020 are another special case. While measurements up to
 566 6 March still keep to the correlation for typical years, data for the rest of March clearly
 567 follow a different trajectory. This is shown by the color scale squares in Figure 5. March
 568 ozone columns decrease more rapidly than expected for temperatures near and below T_{NAT} ,
 569 and this behaviour is consistent across all instruments that have data in March. This
 570 indicates that chemistry was much more dominant than usual. Once chemical depletion
 571 stops in late March, ozone columns start increasing with temperature, but following a
 572 trajectory that is different from the correlation for typical years. The exceptionally long-
 573 lived vortex presents an opportunity to observe this recovery. The trajectory of ozone
 574 columns in April (color scale dots and red dashed lines in Fig. 5a, d) follows a line ap-
 575 proximately parallel to the typical correlation, but with a significant negative offset. This
 576 offset (calculated at $T_{18km} = 210$ K) is 84 DU and 93 DU for the GBS and Brewer datasets,
 577 respectively, and might be interpreted as the approximate amount of additional chemi-
 578 cal ozone destruction in 2020 compared to more typical Arctic winters. While adding
 579 late March data to the linear fits results in a very similar correlation, only April data
 580 were included, for consistency with the ozone loss estimates discussed in Section 3.3. 2011
 581 measurements follow a trajectory similar to 2020 (see also Adams, Strong, Zhao, et al.,
 582 2012). Ozone columns start to clearly deviate from the typical correlation from 13 March
 583 onward. The few late-season measurements in 2011 correspond to the rapid increase of
 584 ozone on 4-6 April (Fig. 1a), and follow a trajectory with a negative ozone offset on the
 585 correlation plots. While direct comparisons are difficult given that the instruments mostly

586 measured outside the vortex after 23 March 2011, the ozone offset in Figure 5a and 5d
 587 is generally larger in 2020 than in 2011. These offsets highlight that chemical ozone de-
 588 struction in both 2011 and 2020 was exceptional in the context of the data record pre-
 589 sented here.

590 Measurements of HF from the Bruker FTIR can be used as another dynamical tracer.
 591 Since HF is long-lived and chemically unreactive, it can be used as a tracer of vertical
 592 motion (Mankin et al., 1990; Toon et al., 1992). HF columns increase when the air col-
 593 umn is descending with replenishment at the top with air from neighbouring columns.
 594 As a result, HF columns are generally larger in the vortex than outside the vortex (Fig.
 595 S1a in the supporting information, hereafter "SI"). HF shows an increasing trend in the
 596 stratosphere (e.g. Griffin et al., 2017), and this trend has been accounted for before scal-
 597 ing with the HF columns (see SI). Inside the vortex, the smallest trend-corrected HF columns
 598 were measured in 2011, 2014, and 2020, and the largest columns were measured in 2015.
 599 This indicates unusually strong descent in 2015, consistent with Manney et al. (2015).
 600 To remove some of the dynamical effects from the Bruker FTIR dataset, we normalized
 601 the measurements of ozone, NO_2 , HCl, ClONO_2 , and HNO_3 with the HF columns (after
 602 Lindenmaier et al., 2012, but with trend-corrected HF columns). The results are shown
 603 in Figure S1b-f in the SI. Since column values of HF and other trace gases would change
 604 in unison if the main driver was dynamics, we assume that any decrease in the HF ra-
 605 tios is largely the result of chemistry. It should be noted that the trend correction changes
 606 the HF columns, but does not substantially impact the year-to-year variability of the HF
 607 ratios described below.

608 The 2020 time series of HF-normalized HCl and ClONO_2 show the same evolution
 609 as the columns in Figure 2c-d, with consistently low values in March, and a gradual in-
 610 crease past 20 March. The 2011 ratios are also similar to the column values, indicating
 611 that the extremely low columns of HCl and ClONO_2 in both years were primarily due
 612 to heterogeneous chemistry, and not variability of transport. The evolution of HF-normalized
 613 HNO_3 follows the same patterns as seen in Figure 2e, but the differences between indi-
 614 vidual years are smaller. The large drop in HNO_3 concentrations on 16-19 March 2020
 615 is still apparent in the HF-normalized time series, confirming that HNO_3 was taken up
 616 on PSC particles. HF-Normalized NO_2 columns show that when accounting for dynam-
 617 ical differences, NO_2 levels were similarly low in 2020 and 2011. The slow increase of NO_2
 618 columns in 2020 is apparent in the HF-normalized time series, in agreement with Fig-
 619 ure 4b.

620 Compared to Figure 1a, the HF-normalized ozone time series tells a very similar
 621 story. HF-Normalized ozone was smaller in 2020 than in any previous year, with the min-
 622 imum values recorded on 26 March (consistent with the Bruker FTIR ozone minima).
 623 Differences between 2020 and other years are reduced in the HF-normalized time series,
 624 as expected since transport generally plays a significant role in maintaining higher ozone
 625 concentrations inside the vortex. The trend-corrected HF columns indicate that verti-
 626 cal motion was likely similar in 2011 and 2020. The fact that HF-normalized ozone still
 627 reached all-time minima in 2020 further highlights the role of chemical ozone depletion.
 628 This is examined in more detail in the next section.

629 3.3 Estimates of Chemical Ozone Loss

630 The narrow altitude region of depleted ozone seen in the ozonesonde profiles (Fig.
 631 1b), the sharp deviations from the typical relationship of ozone and temperature (Fig.
 632 5), and record low HF-normalized ozone all indicate that chemical ozone loss played a
 633 large role in spring 2020. Since our instruments do not measure during the winter (po-
 634 lar night), we have no in-vortex measurements from periods with no chemical ozone de-
 635pletion, and therefore cannot estimate ozone loss from the measurements alone. In order
 636 to quantify chemical ozone loss, we use the passive tracer method. Absolute ozone

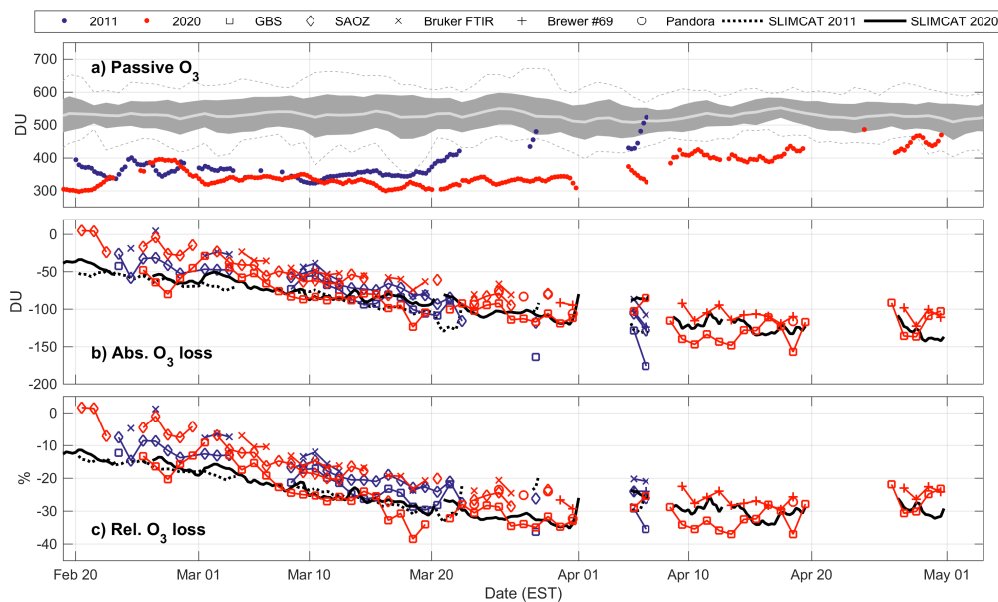


Figure 6. a) SLIMCAT passive ozone. The gray shaded area shows statistics of passive ozone (after Fig. 1) for years when the vortex was not present over Eureka. The colored points show in-vortex data for 2011 and 2020. b) Absolute and c) relative ozone loss inside the vortex for 2011 and 2020, calculated as described in the text. The datapoints show daily average loss for the measurements, and the black lines show 6-hourly values using SLIMCAT active ozone.

637 loss is calculated by subtracting measured ozone from SLIMCAT passive ozone, and rel-
 638 ative ozone loss is calculated as absolute loss over passive ozone. It should be noted that
 639 empirical ozone loss estimates have large uncertainties, and passive subtraction could po-
 640 tentially overestimate ozone loss (Griffin et al., 2019, and references therein).

641 Comparisons between SLIMCAT results and measurements are included in the SI.
 642 SLIMCAT active ozone inside the vortex shows good agreement with all instruments (Fig.
 643 S2, S3), with mean relative differences (SLIMCAT minus measurements) of 1.4%, -3.9%,
 644 -8.9%, and -4.0% for the GBS, SAOZ, Bruker FTIR and Brewer data, respectively (in-
 645 vortext measurements for all years). The larger differences with respect to the Bruker FTIR
 646 dataset are partly due to spatial mismatch in late February (high-SZA measurements,
 647 see SI). HCl and ClONO₂ agree well with Bruker FTIR measurements inside the vortex
 648 (-4.0% and 0.6%, respectively), while HNO₃ columns show a negative bias (-18.1%).
 649 The underestimation of HNO₃ is likely related to the simple equilibrium denitrification
 650 scheme in the model (e.g., Feng et al., 2011). To assess SLIMCAT passive ozone, we used
 651 ozonesonde total columns from December of each year. The mean difference between pas-
 652 sive ozone and the ozonesonde columns is 4.8 ± 9.6 DU ($2.0 \pm 2.7\%$, mean and standard
 653 error) for 2000-2018, indicating that SLIMCAT successfully simulates observed ozone be-
 654 fore chemical depletion starts.

655 The passive ozone time series inside the vortex for 2020 is shown in Figure 6a. Pas-
 656 sive ozone hovered around 300-350 DU for all of March, well below typical springtime
 657 values when the vortex is not present over Eureka (gray shading in Fig. 6a). This indi-
 658 cates that dynamical mechanisms, as discussed above, are in part responsible for the ex-
 659 ceptionally low column values observed in the spring. Passive transport of ozone alone
 660 would have caused a year with ozone minima that were surpassed only by 2011, as in-

661 dicated by the very low values of out-of-vortex ozone measured in early April (gray points
 662 in Fig. 1a). Passive ozone in 2011 was as low as in 2020 until early March, but the two
 663 time series start to diverge after 10 March. Passive ozone in 2011 increased sharply in
 664 late March, and again in early April. These increases correspond well to the increases
 665 in the measured ozone columns (Fig. 1a).

666 Figure 6b-c show daily averages of absolute and relative ozone loss for all the in-
 667 struments. SLIMCAT passive ozone was linearly interpolated to the measurement times,
 668 using only the datapoints that were inside the vortex based on vertical DMPs correspond-
 669 ing to the SLIMCAT ozone columns. Ozone loss values were taken to be inside the vor-
 670 tex only if both the measurement and the corresponding SLIMCAT column were inside
 671 the vortex. In 2020, chemical ozone loss was apparent by the end of February, and its
 672 magnitude gradually increased until the end of March. Loss estimates for individual in-
 673 struments show some scatter, in accordance with the differences between ozone columns
 674 (Sect. 3.1). The GBS instruments measured the lowest ozone column values (Fig 1a),
 675 and therefore differences from passive ozone are most pronounced for this dataset. Ab-
 676 solute differences fell below 100 DU by mid-March, and reached 150 DU in April (max-
 677 imum of 157 DU on 18 April). Relative differences show a similar pattern, with values
 678 well below 30% in the second half of March and in April. The maximum relative differ-
 679 ence of 38% was reached on 18 March. SAOZ measurements are irregular past 14 March,
 680 and the last in-vortex measurement was on 29 March. The maximum difference of 95
 681 DU (29%) occurred on the second to last measurement day, 26 March. Bruker FTIR mea-
 682 surement coverage is weather-dependent, and the in-vortex measurements ended on 26
 683 March. The maximum difference of 81 DU (25%) was reached on that day. Brewer mea-
 684 surements started on 30 March, and consistently measured ozone more than 100 DU smaller
 685 than SLIMCAT passive ozone. The maximum absolute difference of 123 DU occurred
 686 on 28 April, while 29% relative difference was observed on both 31 March and 17 April.
 687 The Pandora instrument has only six days of in-vortex measurements. The maximum
 688 absolute and relative differences of 117 DU and 32% were observed on 18 April and 31
 689 March, respectively.

690 Our loss estimates are generally similar for 2020 and 2011. Results using SLIM-
 691 CAT active ozone (black lines in Fig. 6b, c) show that absolute loss was slightly higher
 692 in 2011. Relative loss was very similar, although ozone loss continued longer (to the end
 693 of March) in 2020, resulting in more overall relative loss. The measurements tell a simi-
 694 lar story. The absolute differences generally overlap for 2011 and 2020, but the peak losses
 695 are greater for 2011. The daily peak loss from the GBS, SAOZ, Bruker FTIR and Brewer
 696 datasets was 176, 129, 108, and 124 DU, respectively, compared to 157, 95, 81, and 123
 697 DU in 2020. Peak relative loss, on the other hand, was smaller in 2011 for all instruments,
 698 with values of 36, 28, 24, and 24%, compared to 38, 29, 25, and 29% in 2020. Overall,
 699 column ozone loss was similar between 2011 and 2020 despite the smaller VMRs reached
 700 in 2020 ozonesonde profiles (Manney et al., 2020; Wohltmann et al., 2020). This is largely
 701 explained by the higher passive ozone simulated by SLIMCAT for 2011 (Fig. 6a).

702 For the spring of 2011, previous studies report a range of ozone loss estimates. Adams,
 703 Strong, Zhao, et al. (2012) and Lindenmaier et al. (2012) used data from Eureka with
 704 methods similar to this paper. Adams, Strong, Zhao, et al. (2012) estimated a mean ozone
 705 loss of 99-108 DU (27-29%) for 12-20 March (GBS and SAOZ data), while Lindenmaier
 706 et al. (2012) estimated 35% for all in-vortex measurements (Bruker FTIR data). The
 707 corresponding values for 2011 in this paper are 92-77 DU (26-21%), and 13%, respec-
 708 tively. The large differences are due in part to the updated chemistry and transport in
 709 the SLIMCAT simulations used here. Adams, Strong, Zhao, et al. (2012) corrected SLIM-
 710 CAT passive ozone to December ozonesonde columns, while Lindenmaier et al. (2012)
 711 did not implement a correction. Given the updated SLIMCAT simulations, and because
 712 of the diversity of methods (and sampling of datasets) used in previous studies, loss es-
 713 timates presented here are not necessarily directly comparable to the literature. Esti-

714 mates of ozone loss from the present dataset are therefore a better basis of comparison.
 715 Using equivalent periods in March for 2011 and 2020, estimates of absolute loss are gen-
 716 erally similar or smaller, while relative loss is greater, in 2020 than in 2011, for all in-
 717 struments. This is consistent with the peak daily loss results discussed above.

718 Quantifying overall chemical ozone loss from a single ground station is challeng-
 719 ing, given the variability of both vortex location and measurement coverage. For the best
 720 estimate, the vortex should be stable, and remain above the station, after chemical ozone
 721 destruction ceased. This was not the case in 2011, while the spring of 2020 fits these re-
 722 quirements best among all winters in the measurement record presented here. Accord-
 723 ing to all indicators (trace gas measurements, correlation of ozone with temperature, SLIM-
 724 CAT simulations), ozone depletion stopped by late March 2020. The GBS and Brewer
 725 instruments measured inside the vortex for the majority of April. Mean ozone loss in April
 726 is then a good indicator of overall chemical ozone loss inside the vortex above Eureka.
 727 The mean loss calculated from the GBS measurements is 127 DU (31%), while the same
 728 value is 111 DU (27%) using measurements from Brewer #69. Some of these differences
 729 are likely related to the different viewing geometries, since DOAS path lengths in the 16-
 730 20 km altitude region are several times longer than those for direct-sun measurements.
 731 Our ozone loss estimate of 111-127 DU (27-31%) is consistent with values of 125-135 DU
 732 from Wohltmann et al. (2020) and Grooß and Müller (2020), who also used the passive
 733 tracer method, but with different chemical transport models.

734 4 Conclusions

735 The unusually cold, strong, and persistent polar vortex in the winter and spring
 736 of 2019/2020 created the greatest potential for ozone depletion ever observed in the Arc-
 737 tic. Accordingly, ozone columns across the Arctic reached record lows, surpassing pre-
 738 vious records set in 2011. The GBS, SAOZ, Bruker FTIR, Pandora, and Brewer instru-
 739 ments at Eureka, Canada all observed record low ozone columns (187, 221, 240, 222, and
 740 218 DU) in their respective time series. Persistent enhancements of BrO and OCIO dSCDs
 741 in the GBS dataset indicate that chlorine activation was ongoing until late March, and
 742 consistently low HCl and ClONO₂ columns from the Bruker FTIR point to heterogeneous
 743 chemistry on PSC particles. HNO₃ columns, on the other hand, were not as low as in
 744 2011, and lower stratospheric temperatures were slightly above T_{NAT} for most of the
 745 spring. This is consistent with a less denitrified stratosphere above Eureka indicated by
 746 the NO₂ measurements. The smallest ozone column values were observed on 16-19 March,
 747 coincident with a significant drop in temperatures and HNO₃ columns. CRL measure-
 748 ments indicated the presence of PSCs (at 14-16 km altitude) during the same period.
 749 Ozonesondes measured ozone mixing ratios below 0.5 ppmv (with minima below 0.2 ppmv)
 750 in the 16-20 km altitude range in late March and throughout April. These values are un-
 751 precedented in the Arctic, and are more similar to values commonly observed in the Antarc-
 752 tic ozone hole. While the vortex remained cold and stable throughout April, chlorine ac-
 753 tivation largely stopped by the end of March, as evidenced by increasing concentrations
 754 of chlorine reservoirs and NO₂.

755 Dynamical contributions to ozone variability must be considered for an accurate
 756 assessment of chemical ozone loss. Passive ozone from the SLIMCAT chemical transport
 757 model indicates that ozone column values in 2020 would likely have been unusually low
 758 even without chemical processing. Ozone columns are usually smaller in cold winters,
 759 and Eureka ozone measurements inside the vortex generally show good correlation with
 760 lower stratospheric temperature. This relationship, however, was substantially different
 761 in 2020 (and in 2011) compared to what is observed for more typical years. This indi-
 762 cates that chemical ozone depletion played an exceptionally large role, and contributed
 763 to significant additional ozone loss, in 2020 when compared to compared to typical Arc-
 764 tic winters. Bruker FTIR measurements normalized by HF total columns confirm the
 765 major role of chemistry in shaping the 2020 trace gas time series.

766 Chemical loss inside the vortex was estimated using measurements at Eureka and
767 SLIMCAT simulations of passive ozone. Using consistent datasets for the entire time se-
768 ries, we showed that all instruments observed smaller daily peak absolute loss in 2020
769 (81-157 DU) than in 2011 (108-176 DU). The absolute loss time series generally over-
770 lap, but the daily peaks were higher in 2011. Daily peak relative loss, on the other hand,
771 was greater in 2020 (25-38%) than in 2011 (24-36%) for all instruments. While overall
772 ozone loss is difficult to estimate from a single ground station due to the variable posi-
773 tion of the vortex, spring 2020 measurements have good coverage inside the vortex af-
774 ter chemical depletion stopped. Using Brewer and GBS measurements throughout April,
775 the mean chemical ozone loss inside the vortex was estimated to be 111-127 DU (27-31%)
776 over Eureka. As the Arctic stratosphere changes in response to climate change, long-term
777 datasets remain essential for assessing unusual springtime conditions and ozone deple-
778 tion. The spring of 2020 was exceptional in the context of the 20-year dataset presented
779 here, but similar (or even more extreme) conditions could arise given the large interan-
780 nual variability of the Arctic vortex and the slow decline of ozone-depleting substances.

781 Acknowledgments

782 The 2006-2020 UT-GBS, PEARL-GBS, SAOZ, Bruker FTIR and CRL measure-
783 ments were made at PEARL by CANDAC. CANDAC has been supported by the At-
784 lantic Innovation Fund/Nova Scotia Research Innovation Trust, Canada Foundation for
785 Innovation, Canadian Foundation for Climate and Atmospheric Sciences (CFCAS), Cana-
786 dian Space Agency (CSA), Environment and Climate Change Canada (ECCC), Gov-
787 ernment of Canada International Polar Year funding, Natural Sciences and Engineer-
788 ing Research Council (NSERC), Northern Scientific Training Program (NSTP), Ontario
789 Innovation Trust, Polar Continental Shelf Program, and Ontario Research Fund. Brewer,
790 Pandora, ozonesonde, and radiosonde measurements were made by ECCC (additional
791 thanks to Michael Brohart, Jonathan Davies, Reno Sit, and Sum Chi Lee). The spring
792 2004-2020 UT-GBS, PEARL-GBS, SAOZ, Bruker FTIR, Brewer, Pandora, CRL, and
793 ozonesonde measurements were also supported by the Canadian Arctic ACE/OSIRIS Val-
794 idation Campaigns, which were funded by CSA, NSERC, NSTP, and ECCC. Spring 2007
795 GBS measurements were also supported by the Centre for Global Change Science. The
796 2001–2003 GBS measurements were supported by CFCAS and NSTP. K. Bogner was
797 partially supported by the NSERC CREATE Training Program in Arctic Atmospheric
798 Science, the Arctic Validation And Training for Atmospheric Research in Space program,
799 funded by CSA, and ECCC’s G&C program. SAOZ participation in the campaigns was
800 supported by the Centre National D’Etudes Spatiales. Work carried out at the Jet Propul-
801 sion Laboratory, California Institute of Technology was done under contract with the
802 National Aeronautics and Space Administration. The SLIMCAT modelling was supported
803 by the NERC SISLAC project (NE/R001782/1). The model simulations were performed
804 on the UK Archer and Leeds ARC HPC machines.

805 The authors wish to thank PEARL site manager Pierre Fogal, the CANDAC op-
806 erators, and the staff at ECCC’s Eureka Weather Station for their contributions to data
807 acquisition, logistics, and on-site support. The authors also wish to thank Matthew Bass-
808 ford, Elham Farahani, Annemarie Fraser, Cristen Adams, and Sophie Tran for their con-
809 tribution to the GBS measurements, as well as Rodica Lindenmaier, Rebecca Batche-
810 lor, Dan Weaver, Joseph Mendonca, Stephanie Conway, Erik Lutsch, Sébastien Roche,
811 and Alistair Duff for their contribution to the Bruker FTIR measurements and retrievals.
812 We thank Manuel Gebetsberger, Daniel Santana Diaz, Martin Tiefengraber and Alexan-
813 der Cede from the Pandonia Global Network (PGN) and Nader Abuhassan from SciGlob
814 for their technical support of Pandora measurements in Eureka.

815 Data availability: UT-GBS and PEARL-GBS ozone and NO₂ data, as well as the
816 Bruker FTIR measurements of ozone, HCl, ClONO₂, HNO₃, and HF are available from
817 the NDACC database at <http://www.ndaccdemo.org/stations/eureka-canada>. The

818 SAOZ ozone and NO₂ data can be found at http://saoz.obs.uvsq.fr/SAOZ_consol
 819 [_v3.html](http://saoz.obs.uvsq.fr/SAOZ_consol_v3.html). Ozone sonde and Brewer measurements are available on the World Ozone and
 820 Ultraviolet Radiation Data Centre (<https://woudc.org/data/explore.php?lang=en>,
 821 Station: Eureka (315)). Radiosonde data are available through the University of Wyoming
 822 Upper Air Database (<http://weather.uwyo.edu/upperair/sounding.html>, Station
 823 Number: 71917). Other datasets, such as the OCIO and BrO dSCDs, the HCl (unfiltered)
 824 and NO₂ measurements from the Bruker FTIR, the corrected Pandora ozone, the CRL
 825 backscatter coefficients, and the SLIMCAT profiles, are available through the Scholars
 826 Portal Dataverse (Bognar et al., 2020). MERRA-2 data used for the DMP calculations
 827 are available at <https://disc.sci.gsfc.nasa.gov/ui/datasets?keywords=%22MERRA>
 828 [-2%22](https://disc.sci.gsfc.nasa.gov/ui/datasets?keywords=%22MERRA).

829 References

- 830 Adams, C., Strong, K., Batchelor, R. L., Bernath, P. F., Brohede, S., Boone, C., ...
 831 Zhao, X. (2012). Validation of ACE and OSIRIS Ozone and NO₂ Measure-
 832 ments Using Ground Based Instruments at 80° N. *Atmospheric Measurement*
 833 *Techniques*, 5(5), 927–953. doi: 10.5194/amt-5-927-2012
- 834 Adams, C., Strong, K., Zhao, X., Bassford, M. R., Chipperfield, M. P., Daffer, W.,
 835 ... Walker, K. A. (2012). Severe 2011 ozone depletion assessed with 11 years
 836 of ozone, NO₂, and OCIO measurements at 80°N. *Geophysical Research Let-*
 837 *ters*, 39(5). doi: 10.1029/2011GL050478
- 838 Adams, C., Strong, K., Zhao, X., Bourassa, A. E., Daffer, W. H., Degenstein, D.,
 839 ... Wohltmann, I. (2013). The spring 2011 final stratospheric warming above
 840 Eureka: anomalous dynamics and chemistry. *Atmospheric Chemistry and*
 841 *Physics*, 13(2), 611–624. doi: 10.5194/acp-13-611-2013
- 842 Balis, D., Isaksen, I. S. A., Zerefos, C., Zyrichidou, I., Eleftheratos, K., Tourpali, K.,
 843 ... Orsolini, Y. (2011). Observed and modelled record ozone decline over the
 844 Arctic during winter/spring 2011. *Geophysical Research Letters*, 38(23). doi:
 845 10.1029/2011GL049259
- 846 Batchelor, R. L., Strong, K., Lindenmaier, R., Mittermeier, R. L., Fast, H., Drum-
 847 mond, J. R., & Fogal, P. F. (2009). A new Bruker IFS 125HR FTIR spec-
 848 trometer for the polar environment atmospheric research laboratory at Eureka,
 849 Nunavut, Canada: measurements and comparison with the existing Bomem
 850 DA8 spectrometer. *Journal of Atmospheric and Oceanic Technology*, 26(7),
 851 1328–1340. doi: 10.1175/2009JTECHA1215.1
- 852 Bernhard, G. H., Fioletov, V. E., Grooß, J.-U., Ialongo, I., Johnsen, B., Lakkala,
 853 K., ... Svendby, T. (2020). Record-Breaking Increases in Arctic So-
 854 lar Ultraviolet Radiation Caused by Exceptionally Large Ozone Depletion
 855 in 2020. *Geophysical Research Letters*, n/a(n/a), e2020GL090844. doi:
 856 <https://doi.org/10.1029/2020GL090844>
- 857 Bognar, K., Alwarda, R., Strong, K., Chipperfield, M. P., Dhomse, S. S., Drum-
 858 mond, J. R., ... Zhao, X. (2020). *Replication data for: Unprecedented spring*
 859 *2020 ozone depletion in the context of 20 years of measurements at Eureka,*
 860 *Canada*. Scholars Portal Dataverse. (V1) doi: 10.5683/SP2/OLZ4PK
- 861 Bognar, K., Zhao, X., Strong, K., Boone, C. D., Bourassa, A. E., Degenstein, D. A.,
 862 ... Zou, J. (2019). Updated validation of ACE and OSIRIS ozone and
 863 NO₂ measurements in the Arctic using ground-based instruments at Eureka,
 864 Canada. *Journal of Quantitative Spectroscopy and Radiative Transfer*, 238,
 865 106571. doi: 10.1016/j.jqsrt.2019.07.014
- 866 Brohede, S., McLinden, C. A., Berthet, G., Haley, C. S., Murtagh, D., & Sioris,
 867 C. E. (2007). A stratospheric NO₂ climatology from Odin/OSIRIS limb-
 868 scatter measurements. *Canadian Journal of Physics*, 85(11), 1253–1274. doi:
 869 10.1139/p07-141
- 870 Cede, A. (2019, October). Manual for Blick Software Suite 1.7 [Computer software

- 871 manual].
- 872 Chipperfield, M. P. (2006). New version of the TOMCAT/SLIMCAT off-line chem-
 873 ical transport model: Intercomparison of stratospheric tracer experiments.
 874 *Quarterly Journal of the Royal Meteorological Society*, *132*(617), 1179–1203.
 875 doi: 10.1256/qj.05.51
- 876 Chipperfield, M. P., Dhomse, S. S., Feng, W., McKenzie, R. L., Velders, G. J. M.,
 877 & Pyle, J. A. (2015). Quantifying the ozone and ultraviolet benefits already
 878 achieved by the Montreal Protocol. *Nature communications*, *6*(1), 1–8. doi:
 879 10.1038/ncomms8233
- 880 Chipperfield, M. P., & Jones, R. L. (1999). Relative influences of atmospheric chem-
 881 istry and transport on Arctic ozone trends. *Nature*, *400*(6744), 551–554. doi:
 882 10.1038/22999
- 883 Coy, L., Nash, E. R., & Newman, P. A. (1997). Meteorology of the polar vortex:
 884 Spring 1997. *Geophysical Research Letters*, *24*(22), 2693–2696. doi: 10.1029/
 885 97GL52832
- 886 DeLand, M. T., Bhartia, P. K., Kramarova, N., & Chen, Z. (2020). OMPS LP
 887 Observations of PSC Variability During the NH 2019-2020 Season. *Geophysical*
 888 *Research Letters*, *47*(20), e2020GL090216. doi: 10.1029/2020GL090216
- 889 Dhomse, S. S., Chipperfield, M. P., Feng, W., Ball, W. T., Unruh, Y. C., Haigh,
 890 J. D., ... Smith, A. K. (2013). Stratospheric O₃ changes during 2001–
 891 2010: the small role of solar flux variations in a chemical transport model.
 892 *Atmospheric Chemistry and Physics*, *13*(19), 10113–10123. doi: 10.5194/
 893 acp-13-10113-2013
- 894 Dhomse, S. S., Feng, W., Montzka, S. A., Hossaini, R., Keeble, J., Pyle, J. A., ...
 895 Chipperfield, M. P. (2019). Delay in recovery of the Antarctic ozone hole from
 896 unexpected CFC-11 emissions. *Nature communications*, *10*(1), 1–12.
- 897 Dunkerton, T. J., & Delisi, D. P. (1986). Evolution of potential vorticity in the win-
 898 ter stratosphere of January-February 1979. *Journal of Geophysical Research:*
 899 *Atmospheres*, *91*(D1), 1199–1208. doi: 10.1029/JD091iD01p01199
- 900 Eyring, V., Waugh, D. W., Bodeker, G. E., Cordero, E., Akiyoshi, H., Austin, J.,
 901 ... Yoshiki, M. (2007). Multimodel projections of stratospheric ozone in the
 902 21st century. *Journal of Geophysical Research: Atmospheres*, *112*(D16). doi:
 903 10.1029/2006JD008332
- 904 Feng, W., Chipperfield, M. P., Davies, S., Mann, G. W., Carslaw, K. S., Dhomse, S.,
 905 ... Santee, M. L. (2011). Modelling the effect of denitrification on polar ozone
 906 depletion for Arctic winter 2004/2005. *Atmospheric Chemistry and Physics*,
 907 *11*(13), 6559–6573. doi: 10.5194/acp-11-6559-2011
- 908 Feng, W., Chipperfield, M. P., Davies, S., von der Gathen, P., Kyrö, E., Volk, C. M.,
 909 ... Belyaev, G. (2007). Large chemical ozone loss in 2004/2005 Arctic win-
 910 ter/spring. *Geophysical Research Letters*, *34*(9). doi: 10.1029/2006GL029098
- 911 Fogal, P. F., LeBlanc, L. M., & Drummond, J. R. (2013). The Polar Environment
 912 Atmospheric Research Laboratory (PEARL): sounding the atmosphere at 80°
 913 North. *Arctic*, *66*(3), 377–386. doi: 10.2307/23594645
- 914 Fraser, A., Adams, C., Drummond, J. R., Goutail, F., Manney, G., & Strong, K.
 915 (2009). The Polar Environment Atmospheric Research Laboratory UV-
 916 visible Ground-Based Spectrometer: First measurements of O₃, NO₂, BrO,
 917 and OClO columns. *Journal of Quantitative Spectroscopy and Radiative Trans-*
 918 *fer*, *110*(12), 986–1004. doi: 10.1016/j.jqsrt.2009.02.034
- 919 Gelaro, R., McCarty, W., Suárez, M. J., Todling, R., Molod, A., Takacs, L., ...
 920 Zhao, B. (2017). The modern-era retrospective analysis for research and ap-
 921 plications, version 2 (MERRA-2). *Journal of Climate*, *30*(14), 5419–5454. doi:
 922 10.1175/JCLI-D-16-0758.1
- 923 GMAO. (2015). MERRA-2 inst3_3d_asm_Nv: 3d,3-Hourly,Instantaneous,Model-
 924 Level,Assimilation,Assimilated Meteorological Fields V5.12.4 [Computer
 925 software manual]. Greenbelt, MD, USA. (Accessed: 2020/08/01) doi:

- 926 10.5067/WWQSQ8IVFW8
 927 Griffin, D., Walker, K. A., Conway, S., Kolonjari, F., Strong, K., Batchelor, R.,
 928 ... Weaver, D. (2017). Multi-year comparisons of ground-based and space-
 929 borne Fourier transform spectrometers in the high Arctic between 2006
 930 and 2013. *Atmospheric Measurement Techniques*, 10(9), 3273–3294. doi:
 931 10.5194/amt-10-3273-2017
- 932 Griffin, D., Walker, K. A., Wohltmann, I., Dhomse, S. S., Rex, M., Chipperfield,
 933 M. P., ... Tarasick, D. (2019). Stratospheric ozone loss in the Arctic winters
 934 between 2005 and 2013 derived with ACE-FTS measurements. *Atmospheric
 935 Chemistry and Physics*, 19(1), 577–601. doi: 10.5194/acp-19-577-2019
- 936 Grooß, J.-U., & Müller, R. (2020). Simulation of the record Arctic stratospheric
 937 ozone depletion in 2020. *Submitted to: Journal of Geophysical Research: Atmo-
 938 spheres*. doi: 10.1002/essoar.10503569.1
- 939 Hendrick, F., Pommereau, J.-P., Goutail, F., Evans, R. D., Ionov, D., Pazmino,
 940 A., ... Van Roozendaal, M. (2011). NDACC/SAOZ UV-visible total ozone
 941 measurements: improved retrieval and comparison with correlative ground-
 942 based and satellite observations. *Atmospheric Chemistry and Physics*, 11(12),
 943 5975–5995. doi: 10.5194/acp-11-5975-2011
- 944 Herman, J., Cede, A., Spinei, E., Mount, G., Tzortziou, M., & Abuhassan, N.
 945 (2009). NO₂ column amounts from ground-based Pandora and MFDOAS
 946 spectrometers using the direct-sun DOAS technique: Intercomparisons and
 947 application to OMI validation. *Journal of Geophysical Research: Atmospheres*,
 948 114(D13). doi: 10.1029/2009JD011848
- 949 Herman, J., Evans, R., Cede, A., Abuhassan, N., Petropavlovskikh, I., & Mc-
 950 Conville, G. (2015). Comparison of ozone retrievals from the Pandora
 951 spectrometer system and Dobson spectrophotometer in Boulder, Col-
 952 orado. *Atmospheric Measurement Techniques*, 8(8), 3407–3418. doi:
 953 10.5194/amt-8-3407-2015
- 954 Hersbach, H., Bell, B., Berrisford, P., Hirahara, S., Hor'anyi, A., Muñoz-Sabater,
 955 J., ... Thépaut, J.-N. (2020). The ERA5 global reanalysis. *Quarterly
 956 Journal of the Royal Meteorological Society*, 146(730), 1999–2049. doi:
 957 10.1002/qj.3803
- 958 Hommel, R., Eichmann, K.-U., Aschmann, J., Bramstedt, K., Weber, M., von Sav-
 959 igny, C., ... Burrows, J. P. (2014). Chemical ozone loss and ozone mini-
 960 hole event during the Arctic winter 2010/2011 as observed by SCIAMACHY
 961 and GOME-2. *Atmospheric Chemistry and Physics*, 14(7), 3247–3276. doi:
 962 10.5194/acp-14-3247-2014
- 963 Inness, A., Chabrillat, S., Flemming, J., Huijnen, V., Langenrock, B., Nicolas, J., ...
 964 Razinger, M. (2020). The unusual 2020 Arctic ozone hole as seen in the CAMS
 965 reanalysis. *Submitted to: Journal of Geophysical Research: Atmospheres*. doi:
 966 10.1002/essoar.10503751.1
- 967 Johansson, S., Santee, M. L., Grooß, J.-U., Höpfner, M., Braun, M., Friedl-Vallon,
 968 F., ... Woiwode, W. (2019). Unusual chlorine partitioning in the 2015/16 Arc-
 969 tic winter lowermost stratosphere: observations and simulations. *Atmospheric
 970 Chemistry and Physics*, 19(12), 8311–8338. doi: 10.5194/acp-19-8311-2019
- 971 Kerr, J. B. (2002). New methodology for deriving total ozone and other atmo-
 972 spheric variables from Brewer spectrophotometer direct sun spectra. *Journal of
 973 Geophysical Research: Atmospheres*, 107(D23), ACH 22-1–ACH 22-17. doi: 10
 974 .1029/2001JD001227
- 975 Kerzenmacher, T. E., Walker, K. A., Strong, K., Berman, R., Bernath, P. F., Boone,
 976 C. D., ... Wu, H. (2005). Measurements of O₃, NO₂ and temperature during
 977 the 2004 Canadian Arctic ACE Validation Campaign. *Geophysical Research
 978 Letters*, 32(16), L16S07. doi: 10.1029/2005GL023032
- 979 Kuttippurath, J., Godin-Beekmann, S., Lefèvre, K., Nikulin, G., Santee, M. L.,
 980 & Froidevaux, L. (2012). Record-breaking ozone loss in the Arctic winter

- 981 2010/2011: comparison with 1996/1997. *Atmospheric Chemistry and Physics*,
 982 12(15), 7073–7085. doi: 10.5194/acp-12-7073-2012
- 983 Lawrence, Z. D., Manney, G. L., & Wargan, K. (2018). Reanalysis intercompar-
 984 isons of stratospheric polar processing diagnostics. *Atmospheric Chemistry and*
 985 *Physics*, 18(18), 13547–13579. doi: 10.5194/acp-18-13547-2018
- 986 Lawrence, Z. D., Perlwitz, J., Butler, A. H., Manney, G. L., Newman, P. A., Lee,
 987 S. H., & Nash, E. R. (2020). The Remarkably Strong Arctic Stratospheric
 988 Polar Vortex of Winter 2020: Links to Record-Breaking Arctic Oscillation
 989 and Ozone Loss. *Journal of Geophysical Research: Atmospheres*, 125(22),
 990 e2020JD033271. doi: 10.1029/2020JD033271
- 991 Lindenmaier, R., Strong, K., Batchelor, R. L., Chipperfield, M. P., Daffer, W. H.,
 992 Drummond, J. R., . . . Walker, K. A. (2012). Unusually low ozone, HCl,
 993 and HNO₃ column measurements at Eureka, Canada during winter/spring
 994 2011. *Atmospheric Chemistry and Physics*, 12(8), 3821–3835. doi:
 995 10.5194/acp-12-3821-2012
- 996 Mankin, W. G., Coffey, M. T., Goldman, A., Schoeberl, M. R., Lait, L. R., & New-
 997 man, P. A. (1990). Airborne measurements of stratospheric constituents over
 998 the Arctic in the winter of 1989. *Geophysical Research Letters*, 17(4), 473-476.
 999 doi: 10.1029/GL017i004p00473
- 1000 Manney, G. L., Daffer, W. H., Zawodny, J. M., Bernath, P. F., Hoppel, K. W.,
 1001 Walker, K. A., . . . Waters, J. W. (2007). Solar occultation satellite data and
 1002 derived meteorological products: Sampling issues and comparisons with Aura
 1003 Microwave Limb Sounder. *Journal of Geophysical Research: Atmospheres*,
 1004 112(D24). doi: 10.1029/2007JD008709
- 1005 Manney, G. L., Froidevaux, L., Santee, M. L., Zurek, R. W., & Waters, J. W.
 1006 (1997). MLS observations of Arctic ozone loss in 1996/97. *Geophysical Re-*
 1007 *search Letters*, 24(22), 2697-2700. doi: 10.1029/97GL52827
- 1008 Manney, G. L., Hegglin, M. I., Daffer, W. H., Santee, M. L., Ray, E. A., Pawson,
 1009 S., . . . Walker, K. A. (2011). Jet characterization in the upper tropo-
 1010 sphere/lower stratosphere (UTLS): applications to climatology and trans-
 1011 port studies. *Atmospheric Chemistry and Physics*, 11(12), 6115–6137. doi:
 1012 10.5194/acp-11-6115-2011
- 1013 Manney, G. L., & Lawrence, Z. D. (2016). The major stratospheric final warming in
 1014 2016: dispersal of vortex air and termination of Arctic chemical ozone loss. *At-*
 1015 *mospheric Chemistry and Physics*, 16(23), 15371–15396. doi: 10.5194/acp-16
 1016 -15371-2016
- 1017 Manney, G. L., Lawrence, Z. D., Santee, M. L., Read, W. G., Livesey, N. J., Lam-
 1018 bert, A., . . . Schwartz, M. J. (2015). A minor sudden stratospheric warm-
 1019 ing with a major impact: Transport and polar processing in the 2014/2015
 1020 Arctic winter. *Geophysical Research Letters*, 42(18), 7808–7816. doi:
 1021 10.1002/2015GL065864
- 1022 Manney, G. L., Livesey, N. J., Santee, M. L., Froidevaux, L., Lambert, A., Lawrence,
 1023 Z., . . . Fuller, R. A. (2020). Record-low Arctic stratospheric ozone in 2020:
 1024 MLS observations of chemical processes and comparisons with previous ex-
 1025 treme winters. *Geophysical Research Letters*, 47(16), e2020GL089063. doi:
 1026 10.1029/2020GL089063
- 1027 Manney, G. L., Santee, M. L., Froidevaux, L., Hoppel, K., Livesey, N. J., & Waters,
 1028 J. W. (2006). EOS MLS observations of ozone loss in the 20042005 Arctic
 1029 winter. *Geophysical Research Letters*, 33(4). doi: 10.1029/2005GL024494
- 1030 Manney, G. L., Santee, M. L., Rex, M., Livesey, N. J., Pitts, M. C., Veeckind, P.,
 1031 . . . Zinoviev, N. S. (2011). Unprecedented Arctic ozone loss in 2011. *Nature*,
 1032 478(7370), 469–475. doi: 10.1038/nature10556
- 1033 Manney, G. L., Zurek, R. W., O’Neill, A., & Swinbank, R. (1994). On the Mo-
 1034 tion of Air through the Stratospheric Polar Vortex. *Journal of the Atmo-*
 1035 *spheric Sciences*, 51(20), 2973–2994. doi: 10.1175/1520-0469(1994)051<2973:

- 1036 OTMOAT\$)2.0.CO;2
- 1037 Marsh, D. R., Mills, M. J., Kinnison, D. E., Lamarque, J.-F., Calvo, N., &
 1038 Polvani, L. M. (2013). Climate change from 1850 to 2005 simulated
 1039 in CESM1 (WACCM). *Journal of climate*, *26*(19), 7372–7391. doi:
 1040 10.1175/JCLI-D-12-00558.1
- 1041 Matthias, V., Dörnbrack, A., & Stober, G. (2016). The extraordinarily strong and
 1042 cold polar vortex in the early northern winter 2015/2016. *Geophysical Research*
 1043 *Letters*, *43*(23), 12,287–12,294. doi: 10.1002/2016GL071676
- 1044 McCullough, E. M., Drummond, J. R., & Duck, T. J. (2019). Lidar measurements
 1045 of thin laminations within Arctic clouds. *Atmospheric Chemistry and Physics*,
 1046 *19*(7), 4595–4614. doi: 10.5194/acp-19-4595-2019
- 1047 McCullough, E. M., Sica, R. J., Drummond, J. R., Nott, G., Perro, C., Thack-
 1048 ray, C. P., ... Walker, K. A. (2017). Depolarization calibration and
 1049 measurements using the CANDAC Rayleigh–Mie–Raman lidar at Eureka,
 1050 Canada. *Atmospheric Measurement Techniques*, *10*(11), 4253–4277. doi:
 1051 10.5194/amt-10-4253-2017
- 1052 McElroy, M. B., Salawitch, R. J., Wofsy, S. C., & Logan, J. A. (1986). Reductions
 1053 of Antarctic ozone due to synergistic interactions of chlorine and bromine. *Nature*,
 1054 *321*(6072), 759–762. doi: 10.1038/321759a0
- 1055 McLinden, C. A., Olsen, S. C., Hannegan, B., Wild, O., Prather, M. J., & Sundet, J.
 1056 (2000). Stratospheric ozone in 3-D models: A simple chemistry and the cross-
 1057 tropopause flux. *Journal of Geophysical Research: Atmospheres*, *105*(D11),
 1058 14653–14665. doi: 10.1029/2000JD900124
- 1059 Molina, L. T., & Molina, M. J. (1987). Production of chlorine oxide (Cl₂O₂) from
 1060 the self-reaction of the chlorine oxide (ClO) radical. *Journal of Physical Chem-*
 1061 *istry*, *91*(2), 433–436. doi: 10.1021/j100286a035
- 1062 Newman, P. A., Gleason, J. F., McPeters, R. D., & Stolarski, R. S. (1997). Anoma-
 1063 lously low ozone over the Arctic. *Geophysical Research Letters*, *24*(22), 2689-
 1064 2692. doi: 10.1029/97GL52831
- 1065 Nott, G. J., Duck, T. J., Doyle, J. G., Coffin, M. E. W., Perro, C., Thackray, C. P.,
 1066 ... Sica, R. J. (2012). A remotely operated lidar for aerosol, temperature, and
 1067 water vapor profiling in the High Arctic. *Journal of Atmospheric and Oceanic*
 1068 *Technology*, *29*(2), 221–234. doi: 10.1175/JTECH-D-11-00046.1
- 1069 Platt, U., & Stutz, J. (2008). *Differential Optical Absorption Spectroscopy*. Springer.
- 1070 Pommereau, J. P., & Goutail, F. (1988). O₃ and NO₂ ground-based measurements
 1071 by visible spectrometry during Arctic winter and spring 1988. *Geophysical Re-*
 1072 *search Letters*, *15*(8), 891–894. doi: 10.1029/GL015i008p00891
- 1073 Pommereau, J.-P., Goutail, F., Lefèvre, F., Pazmino, A., Adams, C., Dorokhov, V.,
 1074 ... van Roozendaal, M. (2013). Why unprecedented ozone loss in the Arctic
 1075 in 2011? Is it related to climate change? *Atmospheric Chemistry and Physics*,
 1076 *13*(10), 5299–5308. doi: 10.5194/acp-13-5299-2013
- 1077 Pougatchev, N. S., Connor, B. J., & Rinsland, C. P. (1996). Infrared measurements
 1078 of the ozone vertical distribution above Kitt Peak. *Journal of Geophysical Re-*
 1079 *search: Atmospheres*, *100*(D8), 16689–16697. doi: 10.1029/95JD01296
- 1080 Rex, M., Salawitch, R. J., Deckelmann, H., von der Gathen, P., Harris, N. R. P.,
 1081 Chipperfield, M. P., ... Zerefos, C. (2006). Arctic winter 2005: Implications
 1082 for stratospheric ozone loss and climate change. *Geophysical Research Letters*,
 1083 *33*(23). doi: 10.1029/2006GL026731
- 1084 Rex, M., Salawitch, R. J., von der Gathen, P., Harris, N. R. P., Chipperfield, M. P.,
 1085 & Naujokat, B. (2004). Arctic ozone loss and climate change. *Geophysical*
 1086 *Research Letters*, *31*(4). doi: 10.1029/2003GL018844
- 1087 Rodgers, C. D. (2000). *Inverse Methods for Atmospheric Sounding: Theory and*
 1088 *Practice* (Vol. 2). World Scientific.
- 1089 Rothman, L. S., Gordon, I. E., Barbe, A., Benner, D. C., Bernath, P. F., Birk, M.,
 1090 ... Vander Auwera, J. (2009). The HITRAN 2008 molecular spectroscopic

- 1091 database. *Journal of Quantitative Spectroscopy and Radiative Transfer*, 110(9-
1092 10), 533–572. doi: 10.1016/j.jqsrt.2009.02.013
- 1093 Salawitch, R. J., Gobbi, G. P., Wofsy, S. C., & McElroy, M. B. (1989). Denitrifica-
1094 tion in the Antarctic stratosphere. *Nature*, 339(6225), 525–527. doi: 10.1038/
1095 339525a0
- 1096 Salby, M. L., & Callaghan, P. F. (2007). On the wintertime increase of Arctic ozone:
1097 Relationship to changes of the polar-night vortex. *Journal of Geophysical Re-
1098 search: Atmospheres*, 112(D6). doi: 10.1029/2006JD007948
- 1099 Singleton, C. S., Randall, C. E., Chipperfield, M. P., Davies, S., Feng, W., Bevilac-
1100 qua, R. M., . . . Harvey, V. L. (2005). 2002–2003 Arctic ozone loss deduced
1101 from POAM III satellite observations and the SLIMCAT chemical trans-
1102 port model. *Atmospheric Chemistry and Physics*, 5(3), 597–609. doi:
1103 10.5194/acp-5-597-2005
- 1104 Singleton, C. S., Randall, C. E., Harvey, V. L., Chipperfield, M. P., Feng, W.,
1105 Manney, G. L., . . . Hoppel, K. W. (2007). Quantifying Arctic ozone loss
1106 during the 20042005 winter using satellite observations and a chemical trans-
1107 port model. *Journal of Geophysical Research: Atmospheres*, 112(D7). doi:
1108 10.1029/2006JD007463
- 1109 Sinnhuber, B.-M., Stiller, G., Ruhnke, R., von Clarmann, T., Kellmann, S., & As-
1110 chmann, J. (2011). Arctic winter 2010/2011 at the brink of an ozone hole.
1111 *Geophysical Research Letters*, 38(24). doi: 10.1029/2011GL049784
- 1112 Solomon, S., Garcia, R. R., Rowland, F. S., & Wuebbles, D. J. (1986). On the deple-
1113 tion of Antarctic ozone. *Nature*, 321(6072), 755–758. doi: 10.1038/321755a0
- 1114 Solomon, S., Haskins, J., Ivy, D. J., & Min, F. (2014). Fundamental differences
1115 between Arctic and Antarctic ozone depletion. *Proceedings of the National
1116 Academy of Sciences*, 111(17), 6220–6225. doi: 10.1073/pnas.1319307111
- 1117 Strahan, S. E., Douglass, A. R., & Newman, P. A. (2013). The contributions of
1118 chemistry and transport to low arctic ozone in March 2011 derived from Aura
1119 MLS observations. *Journal of Geophysical Research: Atmospheres*, 118(3),
1120 1563–1576. doi: 10.1002/jgrd.50181
- 1121 Tarasick, D. W., Davies, J., Smit, H. G. J., & Oltmans, S. J. (2016). A re-evaluated
1122 Canadian ozonesonde record: measurements of the vertical distribution of
1123 ozone over Canada from 1966 to 2013. *Atmospheric Measurement Techniques*,
1124 9(1), 195–214. doi: 10.5194/amt-9-195-2016
- 1125 Tegtmeier, S., Rex, M., Wohltmann, I., & Krüger, K. (2008). Relative importance of
1126 dynamical and chemical contributions to Arctic wintertime ozone. *Geophysical
1127 Research Letters*, 35(17). doi: 10.1029/2008GL034250
- 1128 Tilmes, S., Müller, R., Engel, A., Rex, M., & Russell III, J. M. (2006). Chemical
1129 ozone loss in the Arctic and Antarctic stratosphere between 1992 and 2005.
1130 *Geophysical Research Letters*, 33(20). doi: 10.1029/2006GL026925
- 1131 Toon, G. C., Farmer, C. B., Schaper, P. W., Lowes, L. L., Norton, R. H., Schoe-
1132 berl, M. R., . . . Newman, P. A. (1992). Evidence for subsidence in the 1989
1133 Arctic winter stratosphere from airborne infrared composition measurements.
1134 *Journal of Geophysical Research: Atmospheres*, 97(D8), 7963–7970. doi:
1135 10.1029/91JD03115
- 1136 Tung, K.-K., Ko, M. K. W., Rodriguez, J. M., & Sze, N. D. (1986). Are Antarctic
1137 ozone variations a manifestation of dynamics or chemistry? *Nature*, 322(6082),
1138 811–814. doi: 10.1038/322811a0
- 1139 Tzortziou, M., Herman, J. R., Cede, A., & Abuhassan, N. (2012). High precision,
1140 absolute total column ozone measurements from the Pandora spectrometer
1141 system: Comparisons with data from a Brewer double monochromator and
1142 Aura OMI. *Journal of Geophysical Research: Atmospheres*, 117(D16). doi:
1143 10.1029/2012JD017814
- 1144 WMO. (1957). Meteorology – A three-dimensional science: Second session of the
1145 commission for aerology. *WMO Bulletin*, 4(4), 134–138.

- 1146 WMO. (2014). *Scientific Assessment of Ozone Depletion: 2014*. Geneva, Switzer-
1147 land: Global Ozone Research and Monitoring Project Report 55.
- 1148 WMO. (2018). *Scientific Assessment of Ozone Depletion: 2018*. Geneva, Switzer-
1149 land: Global Ozone Research and Monitoring Project Report 58.
- 1150 Wohltmann, I., von der Gathen, P., Lehmann, R., Maturilli, M., Deckelmann, H.,
1151 Manney, G. L., . . . Rex, M. (2020). Near-Complete Local Reduction of Arctic
1152 Stratospheric Ozone by Severe Chemical Loss in Spring 2020. *Geophysical*
1153 *Research Letters*, *47*(20), e2020GL089547. doi: 10.1029/2020GL089547
- 1154 Zhao, X., Fioletov, V., Brohart, M., Savastiouk, V., Abboud, I., Ogyu, A., . . .
1155 McLinden, C. (2020). The world Brewer reference triad–updated performance
1156 assessment and new double triad. *Atmospheric Measurement Techniques*
1157 *Discussions*, 1–34. doi: 10.5194/amt-2020-324
- 1158 Zhao, X., Fioletov, V., Cede, A., Davies, J., & Strong, K. (2016). Accuracy, pre-
1159 cision, and temperature dependence of Pandora total ozone measurements
1160 estimated from a comparison with the Brewer triad in Toronto. *Atmospheric*
1161 *Measurement Techniques*, *9*(12), 5747–5761. doi: 10.5194/amt-9-5747-2016
- 1162 Zhao, X., Strong, K., Adams, C., Schofield, R., Yang, X., Richter, A., . . . Koo, J.-H.
1163 (2016). A case study of a transported bromine explosion event in the Canadian
1164 high arctic. *Journal of Geophysical Research: Atmospheres*, *121*(1), 457–477.
1165 doi: 10.1002/2015JD023711